LONP1-mediated mitochondrial quality control safeguards metabolic shifts in heart development

Ke Zhao[1], Xinyi Huang[1], Wukui Zhao[1], Bin Lu[2] and Zhongzhou Yang[1&]

[1]State Key Laboratory of Pharmaceutical Biotechnology, MOE Key Laboratory of Model Animal for Disease Study, Model Animal Research Center, and Jiangsu Key Laboratory of Molecular Medicine, Nanjing University Medical School, Nanjing 210093, China.
[2]Department of Biochemistry and Molecular Biology, School of Basic Medical Sciences, Hengyang Medical School, University of South China, Hengyang, Hunan, 421001, China.

[&]Correspondence: Zhongzhou Yang, E-mail: zhongzhouyang@nju.edu.cn; Telephone, +86 25 8359 2264; Bin Lu, E-mail: lubinmito@usc.edu.cn

Keywords: LONP1; mitochondrial quality control; ATF4; glycolysis; oxidative phosphorylation; metabolic shift; heart development

Summary statement: LONP1, an important mitochondrial quality control protein, plays pivotal role in maintaining shift from anaerobic glycolysis to oxidative phosphorylation during heart development, which gives us new perspective on the relationship between mitochondria and heart development.

ABSTRACT

The mitochondrial matrix AAA^+ Lon protease (LONP1) degrades misfolded or unassembled proteins, which play a pivotal role in mitochondrial quality control. During heart development, a metabolic shift from anaerobic glycolysis to mitochondrial oxidative phosphorylation takes place, and this process relies highly on functional mitochondria. However, the relationship between mitochondrial quality control machinery and metabolic shifts is elusive. Here, we interfered with mitochondrial quality control by inactivating *Lonp1* in embryonic cardiac tissue and found severely impaired heart development, leading to embryonic lethality. Mitochondrial swelling, cristae loss and abnormal protein aggregates were evident in the mitochondria of *Lonp1*-deficient cardiomyocytes. Accordingly, the p-eIF2α-ATF4 pathway was triggered, and nuclear translocation of ATF4 was observed. We further demonstrated that ATF4 negatively regulates the expression of *Tfam* while promoting that of *Glut1*, which was responsible for the disruption of the metabolic shift to oxidative phosphorylation. Meanwhile, elevated levels of reactive oxygen species were observed in *Lonp1* mutant cardiomyocytes. This study revealed that LONP1 safeguards metabolic shifts in the developing heart by controlling mitochondrial protein quality and implies that disrupted mitochondrial quality control may cause prenatal cardiomyopathy.

INTRODUCTION

During mammalian embryogenesis, the heart is the first organ to develop and function (Olson and Srivastava, 1996; Harvey, 2002; Bruneau, 2020). Initially, heart tissues form under hypoxic conditions before embryonic day 11.5 (E11.5), and hypoxia inducing factor α (HIFα) drives an anaerobic glycolysis program to provide energy through transcriptional mechanisms for early heart development (Guimarães-Camboa et al., 2015; Menendez-Montes et al., 2016; Maroli and Braun, 2021). From E11.5 onward, a metabolic shift from anaerobic glycolysis to mitochondrial oxidative phosphorylation (oxidative metabolism) takes place in cardiomyocytes, which is

essential for myocardial development (Lopaschuk and Jaswal, 2010; Zhao et al., 2019; Maroli and Braun, 2021). Recently, we identified the chromatin remodeling complex of SRCAP as a pivotal regulator to propel mitochondrial oxidative metabolism for this type of metabolic shift/transition (Xu et al., 2021). Through transcriptional regulation, the SRCAP complex controls mitochondrial maturation morphologically and functionally to meet the energy requirement for rapidly growing myocardium.

In the mitochondria, several distinct quality control machineries monitor the proteome that contains approximately 1500 proteins to safeguard mitochondrial functions (Fischer et al., 2012; Rugarli and Langer, 2012; Song et al., 2021). AAA^+ Lon protease (LONP1) is located in the mitochondrial matrix and functions to degrade misfolded proteins and prevent protein aggregation (Suzuki et al., 1994; Lu et al., 2013; Song et al., 2021). Under stress conditions, LONP1 can directly remove mitochondrial proteins, for instance, the components of the respiratory chain complexes and of the tricarboxylic acid (TCA) cycle, to sustain mitochondrial function (Song et al., 2021). There is also growing evidence to show that LONP1 acts as a chaperone to modulate mitochondrial DNA (mtDNA) stability (Chen et al., 2008; Matsushima et al., 2010; Kao et al., 2015). Thus, LONP1 plays a large role in governing mitochondrial protein folding and removing damaged proteins and therefore participates in mitochondrial quality control.

When cells are subjected to stresses, such as amino acid deprivation, viral infection, heme loss or endoplasmic reticulum (ER) stress, the integrated stress response (ISR) is elicited (Pakos-Zebrucka et al., 2016). Cellular stresses provoke a remarkable elevation of phosphorylated eukaryotic initiation factors 2α (p-eIF2α), further leading to an increase in translation of the master regulator of ISR, activating transcription factor 4 (ATF4) (Jousse et al., 2003; Lu et al., 2004; Dara et al., 2011). ATF4 stimulates a transcriptional program to regulate protein synthesis, unfolded protein response (UPR), autophagy and metabolism (Vattem and Wek, 2004; Kilberg et al., 2009; B'Chir et al., 2013). A recent study indicated that mitochondrial morphological damage and/or dysfunction gives rise to mitochondrial stress and causes the accumulation of ATF4 (Quirós et al., 2017). Mitochondrial stress also promotes

decreased mitochondrial ribosomal proteins (MRPs) to attenuate protein translation (Quirós et al., 2017).

Global deletion of *Lonp1* in mice causes embryonic lethality at E8.5, and knockout embryos exhibit a decline in mtDNA copy number (Quiros et al., 2014). To address whether mitochondrial quality control plays a role in organogenesis and in the surveillance of mitochondrial metabolic shifts, we abolished *Lonp1* in embryonic cardiac tissues. *Lonp1* deficiency caused severely defective heart development and embryonic lethality. Aggregates were evident in the mitochondria of *Lonp1* deletion cardiomyocytes. Accordingly, the accumulation of AFT4 was shown to suppress the expression of *Tfam*- and mtDNA-encoded components of respiratory chain complexes but to enhance the expression of glycolysis regulatory genes, including *Glut1*, resulting in a disrupted metabolic shift during cardiac development.

RESULTS

Lonp1 deficiency in cardiac progenitors impaired ventricular development

We examined the protein level of LONP1 in the developing heart tissue at different stages, and the results indicated a slight but significant enhancement from E10.5 to E12.5 (Fig. S1A and S1B). During this period, the anaerobic glycolysis regulatory protein GLUT1 showed a great reduction and almost disappeared by E12.5 (Fig. S1A). Meanwhile, the mitochondrial oxidative metabolic protein NDUFB8, a component of respiratory chain complex I (CI), displayed a profoundly increased level (Fig. S1A). These results manifest a metabolic shift from anaerobic glycolysis to mitochondrial oxidative phosphorylation from E10.5 to E13.5 and suggest that LONP1 may participate in the metabolic shift.

To understand whether LONP1 is involved in heart development, we first deleted *Lonp1* in the cardiac progenitors of the second heart field that contributes to the development of the cardiac outflow tract (OFT) and the right ventricle (RV). The *Lonp1* deletion mice (*Mef2c-AHF-Cre; Lonp1*$^{F/F}$) showed comparable heart morphology with the control at E9.5 (Fig. 1A), and ISL1 staining for cardiac

progenitors revealed a normal distribution of progenitor cells (Fig. 1B). Furthermore, we observed normal OFT morphogenesis and septation (Fig. S2). Thus, *Lonp1* deficiency does not affect cardiac progenitor development.

However, the *Lonp1* deletion mice showed reduced RV size starting from E11.5, and RV hypoplasia was more prominent from E12.5 to E18.5 (Fig. 1C and 1D). Interestingly, *Lonp1* deletion mice showed increased LV size starting from E14.5 (Fig. 1E). Although the *Lonp1* deletion mice could be born, all of them were lost at postnatal day 0 (P0). The hearts of the *Lonp1* deletion mice manifested enlargement of the two atria and a small RV at birth, indicating heart failure (Fig. 1F).

TUNEL staining was performed to test cell death, and the results showed no obvious apoptosis signal in *Mef2c-AHF-Cre; Lonp1*$^{F/F}$ hearts (Fig. 1G). In contrast, knockout of *Lonp1* led to a significant decrease in cardiac cell proliferation (Fig. 1H). Further study revealed that the cells with reduced proliferation were primarily cardiomyocytes (Fig. 1I).

Overall, deletion of *Lonp1* has little effect on cardiac progenitor development but impairs cardiomyocyte proliferation in the RV.

Deletion of *Lonp1* in cardiomyocytes caused poorly developed myocardium

Lonp1 deficiency in cardiac progenitors impeded cardiomyocyte proliferation in the RV. To confirm this phenotype, we deleted *Lonp1* in embryonic cardiomyocytes using *cTnT-Cre* mice to generate *cTnT-Cre; Lonp1*$^{F/F}$ mice (cardiomyocyte-specific *Lonp1* deletion mice). Similar to *Lonp1* deletion in cardiac progenitors, there was no large change in OFT development or progenitor cell contribution in the hearts of cardiomyocyte-specific *Lonp1* deletion mice (Fig. 2A and 2B). However, these mice started to demonstrate reduced ventricular volume from E11.5 and thinned ventricular wall at E14.5 (Fig. 2C-E) and could not survive after E16.5 (Fig. 2F). The TUNEL assay did not reveal increased apoptotic cardiomyocytes (Fig. 2G). Cell proliferation analysis indicated significantly reduced cardiomyocyte proliferation in an early stage of cardiac development (Fig. 2H).These results confirmed the essential role of LONP1 in embryonic cardiomyocyte development.

Lonp1 deficiency caused mitochondrial abnormalities, increased ROS production and DNA damage

LONP1 is primarily located in the mitochondrial matrix. To determine whether deletion of *Lonp1* had an effect on mitochondrial morphology, we isolated cardiomyocytes from the hearts of control and *cTnT-Cre; Lonp1*$^{F/F}$ mice and cultured them *in vitro*. Afterwards, we examined the mitochondria and found that there was a dramatic morphologic difference between control and *Lonp1*-deficient cardiomyocytes. While the mitochondria in control cardiomyocytes showed a slender network, those in *Lonp1* deletion cardiomyocytes manifested aggregated lamellar structures (Fig. S3). Next, we performed transmission electron microscopy (TEM) analysis to study the mitochondria in the hearts of control and *Lonp1*-deficient mice. The results showed accumulation of high electron density substances in the cardiomyocytes of the *cTnT-Cre; Lonp1*$^{F/F}$ mice (Fig. 3A-F). Meanwhile, the mitochondria in the *Lonp1* mutant cardiomyocytes swelled with disappeared cristae (Fig. 3D-F). Compared with the control group, the damage of mitochondria in different degrees increased significantly in cardiomyocytes of the *cTnT-Cre; Lonp1*$^{F/F}$ mice (Fig. 3G; Ctrl: 0.01167 ± 0.008731 vs cKO: 0.1947 ± 0.04107).

Severe mitochondrial abnormalities could trigger the increased production of reactive oxidative species (ROS). We indeed observed substantially enhanced levels of ROS in *Lonp1* mutant cardiomyocytes (Fig. 3H and 3I). High levels of ROS suppress cell cycle progression, and we found that the mRNA levels of *Cdkn1a* and *Ddit3* were significantly increased in cKO hearts (Fig. 3J), suggesting inhibition of the cell cycle. Meanwhile, we observed a remarkably increased level of γH2A. X, a DNA damage marker in *Lonp1* mutant cardiomyocytes (Fig. 3K and 3L).

Taken together, these results demonstrate that *Lonp1* deletion caused mitochondrial abnormalities, increased ROS production and DNA damage.

Altered metabolic pattern in the *Lonp1* deficient heart

As shown in Fig. 2C, deletion of *Lonp1* impaired heart development starting at E11.5, a developmental stage when a metabolic shift takes place from anaerobic glycolysis to mitochondrial oxidative phosphorylation. To determine whether *Lonp1* deficiency affects the metabolic shift, we examined the metabolic pattern in the hearts of control and *Lonp1* mutant mice. Western blot analysis showed that as early as E11.5, the protein levels of the respiratory chain complex I (CI) component NDUFB8 and the CIV component mitochondrial (mt)-COX2 were reduced significantly compared to those of the control (Fig. S4A and S4B). At E12.5, the protein levels of the CIV component COX4 and the CV component ATP5a1 were substantially decreased compared to those of the control (Fig. 4A and 4B). IF staining also confirmed a significant reduction in NDUFB8 in *Lonp1* mutant cardiomyocytes (Fig. S4C).

In contrast, we observed markedly enhanced protein levels of GLUT1 and GLUT4 in the hearts of *Lonp1*-deficient mice (Fig. 4C-E; Fig. S4D). In addition, the transcript levels of *Glut1*, *Glut4*, and *Hk2* were also elevated in the hearts of *Lonp1*-deficient mice compared to control mice in a HIF1-independent manner (Fig. S4E-I).

Phosphorylation of AMPK can represent tissue energy balance, and we found a substantial increase in phosphor-AMPK levels in the *Lonp1* mutant hearts compared to the control hearts, indicating an energy shortage (Fig. 4F and G).

Taken together, these results demonstrate that a relatively high level of glycolysis takes place in the *Lonp1* mutant heart, suggesting a disrupted metabolic shift.

***Lonp1* deficiency activated ATF4 expression**

We performed RNA-seq using RNA isolated from control and *Lonp1* mutant heart tissues. By comprehensive alignment analysis of the altered genes and Gene Ontology (GO) analysis, we found that *Atf4* was highly expressed in *Lonp1* mutant hearts (Fig. 5A). Quantitative RT–PCR analysis confirmed significantly elevated mRNA levels of *Atf4* in *Lonp1* mutant hearts compared to control hearts at both E10.5 and E12.5 (Fig. 5B). Western blot analysis also showed a marked increase in AFT4 protein levels in *Lonp1* mutant hearts (Fig. 5C and 5D). Through IF staining, we clearly observed

increased expression of ATF4 in both the nucleus and cytoplasm from E10.5 to E12.5 (Fig. 5E and Fig. S5A). Accordingly, the downstream target genes of ATF4 (*Pck2*, *Phgdh*, *Shmt2*, *Pc,* etc.) showed significant enhancement of the expression level (Fig. S5B-D). Meanwhile, we found elevated phosphorylation levels of eIF2α in the *Lonp1* mutant hearts (Fig. 5F and G).

Collectively, our results demonstrate a substantial increase in ATF4 levels and implicate that this type of enhancement is related to elevated phosphorylation of eIF2α.

Reduced protein levels of TFAM and mtDNA-encoded components of respiratory chain complexes in *Lonp1* mutant hearts

Mitochondrial respiratory chain complex components are coordinately encoded by nuclear and mitochondrial DNA (mtDNA), respectively. Gene expression analysis revealed that the mRNA levels of mitochondrial respiratory chain complex components encoded by nuclear DNA were not significantly changed (Fig. 6A). However, we found that the mRNA levels of respiratory chain complex components encoded by mtDNA (*mt-Cox2* and *mt-Atp6*) were significantly decreased in *Lonp1* mutant hearts compared to control hearts (Fig. 6A and Fig. S6A). A previous study with global *Lonp1* deletion mice detected decreased mtDNA copy number (Quiros et al., 2014). Therefore, we checked the total amount of mtDNA in *Lonp1* mutant hearts and found a substantial reduction (Fig. 6B). As the most abundant mtDNA binding protein, mitochondria-associated transcription factor A (TFAM) regulates mtDNA replication and transcription (Matsushima et al., 2010). We therefore examined the level of TFAM, and the results showed a profound decrease in the *Lonp1* mutant hearts (Fig. 6C and 6D). Accordingly, the protein levels of mtDNA-encoded respiratory chain complex Ⅰ component (CI-mt-ND1), complex Ⅳ component (CIV-mt-COX2) and complex Ⅴ component (CV-mt-ATP6) were all significantly decreased in *Lonp1* mutant hearts compared to control hearts (Fig. 6D and 6E).

Furthermore, we found that the reduction of TFAM and mtDNA-encoded respiratory chain complex components in the *Lonp1* mutant heart did not occur at E10.5 but at E11.5 (Fig. S6B-E).

Taken together, *Lonp1* deficiency results in reduced protein levels of TFAM and mtDNA-encoded components of respiratory chain complexes.

ATF4 suppressed the expression of *Tfam* but promoted that of *Glut1*

Next, we constructed inducible *Lonp1*-deficient MEFs derived from *ERt2; Lonp1*$^{F/F}$ mice. Upon 4-OH tamoxifen administration, we found that MEFs without *Lonp1* showed abnormal mitochondrial morphological alterations (Fig. S7A), which was consistent with the results in *Lonp1*-deficient cardiomyocytes (Fig. S3). MEFs lacking *Lonp1* also showed a decrease in the expression level of respiratory chain complex components CI-NDUFB8 and CIV-mt-COX2 but an increase in glycolysis regulatory proteins (Fig. 7A and B). In addition, we found an increase in ATF4 protein levels and a decrease in TFAM protein levels in MEFs lacking *Lonp1* (Fig. 7B). qPCR results showed that the changes in the transcription levels of these genes were consistent with those in *Lonp1* mutant hearts (Fig. 7C). Accordingly, decreased mtDNA copy number was also observed in *Lonp1*-deficient MEFs (Fig. 7D). The p-eIF2α level was enhanced in *Lonp1*-deficient MEFs (Fig. 7E). We observed similar alterations in different cell lines of human 293T cells (Fig. 7F) and rat H9C2 cells (Fig. S7B), suggesting conserved regulation across different species or cell types.

Furthermore, we overexpressed ATF4 (ATF4 OE) in several cell lines. Overexpression of ATF4 did not affect the expression level of LONP1 but was sufficient to reduce that of TFAM (Fig. 7G and Fig. S7C) and led to decreased levels of respiratory chain complex components (Fig. 7G). Accordingly, the ATF4 OE groups showed a lower mtDNA copy number (Fig. 7H). In addition, we observed a decrease in the *Tfam* transcription level but an increase in the *Glut1* transcription level in *Lonp1* knockdown cells and ATF4 OE cells (Fig. 7I). ATF4 positively or negatively regulates target gene expression by binding to the cAMP response element (CRE) sequences proximal to the promoter regions of the target gene (Koyanagi et al.,

2011). We identified the CRE sequences in the promoters of both *Tfam* and *Glut1* and constructed luciferase reporters. A luciferase reporter assay revealed that ATF4 activated the promoter activity of *Glut1* but repressed the promoter activity of *Tfam* (Fig. 7J and 7K). Collectively, these results demonstrate that ATF4 directly represses the transcription of *Tfam* but activates the transcription of *Glut1*.

Pharmacological inhibition of LONP1 activated ATF4

To further understand the relationship between *Lonp1* deficiency and AFT4 activation, we administered CDDO, a well-established LONP1 inhibitor, to cells to mimic *Lonp1* deletion (Bernstein et al., 2012; Zurita Rendon and Shoubridge, 2018; Shin et al., 2021). We first tested the dosage effect of CDDO on cell proliferation and found that at doses ranging from 1.5 to 2.5 μM, CDDO significantly decreased the proliferative capacity of the cells (Fig. S8A-C). Meanwhile, CDDO treatment dramatically reduced the protein levels of respiratory chain complex components (Fig. 8A and Fig. S8D). We also observed the accumulation of ATF4 but a reduction in TFAM, CIV-COX4 and CV-mt-APT6 in a time course-dependent manner (Fig. 8B). Treatment of cells with CDDO (2.5 μM) for 10 hours caused substantially enhanced mRNA and protein levels of ATF4 but remarkably decreased mRNA levels of *Tfam* (Fig. 8C-E). CDDO administration was sufficient to change mitochondrial morphology and to augment the level of ROS (Fig. S8E).

DISCUSSION

Although mitochondrial abnormalities can cause heart developmental defects, the importance of mitochondrial quality control for prenatal heart development has not been well documented. Our study emphasized that the mitochondrial matrix protease LONP1, as a key element in controlling mitochondrial quality control, played a critical role in embryonic heart development. In combination with mouse genetics and pharmacological treatment, we demonstrated that LONP1-mediated mitochondrial

quality control safeguarded the metabolic shift during heart development to meet the energy demands of the growing myocardium and embryonic body.

We identified AFT4 as an important mediator of abolished mitochondrial quality control. Disruption of mitochondrial quality control resulted in a profound accumulation of ATF4, probably as a consequence of activation of the ISR-p-eIF2α signaling pathway, which is consistent with a previous study (Quirós et al., 2017).

Here, we determined that TFAM is a pivotal target gene of ATF4. A cAMP response element (CRE) was discovered in the promoter region of *Tfam,* and a biochemical study demonstrated that ATF4 negatively regulates *Tfam* transcription. Consequently, the expression of several mtDNA-encoded respiratory chain complex components was greatly suppressed after ATF4 activation, which in turn hindered mitochondrial oxidative metabolism. Meanwhile, we found that the key anaerobic glycolysis gene *Glut1* is another target gene of ATF4. Through direct regulation, ATF4 triggers *Glut1* transcription and augments glycolysis. Thus, ATF4 exerts bilateral effects on metabolic regulation. On the one hand, ATF4 suppresses mitochondrial oxidative metabolism through inhibition of TFAM activity, and on the other hand, ATF4 boosts glycolysis by activating *Glut1* expression. The detailed working model of LONP1-mediated mitochondrial quality control in safeguarding metabolic shifts is presented in Fig. 9.

From this study, two important conclusions could be drawn: 1. Mitochondrial quality control is essential for heart development; 2. Mitochondrial quality control safeguards metabolic shifts during heart development. LONP1 connects mitochondrial quality control with metabolic shifts to ensure an energy supply for embryonic heart development.

MATERIALS AND METHODS

Mice

We used *Lonp1*-floxed, *Mef2c-AHF-Cre*, *cTnT-Cre*, *ctTA-Cre* and *ERt2-Cre* (from The Jackson Laboratory, Stock No:008463) mice in this study. All mouse strains were maintained on a C57BL/6 genetic background. Mice were group-housed in accordance with the regulations on mouse welfare and ethics of Nanjing University, with 12 h/12 h light-dark cycles and *ad libitum* access to food and water. The Institutional Animal Care and Use Committee (IACUC) of Model Animal Research Center of Nanjing University approved all animal procedures used in this study.

IF staining

Four percent paraformaldehyde (PFA)-fixed embryos and hearts were dehydrated and embedded in paraffin. Eight-micrometer-thick sections were cut by a Leica RM2016 microtome and then deparaffinized in xylene. We used decreasing concentrations of ethanol to rehydrate the sections and then stained them with hematoxylin and eosin (H&E).

Four percent PFA-fixed embryos and hearts were dehydrated and embedded in OCT medium. Eight-micrometer-thick sections were cut by a Leica CM1950 automated cryostat. For IF staining, we placed sections at room temperature for 20 minutes, washed sections in PBS, used goat serum to block sections and incubated sections in primary antibodies overnight at 4 °C. The next day, we washed the sections with PBS and incubated the sections with secondary antibody for 2 hours. Finally, the sections were washed again and sealed with 50% glycerol before confocal imaging. Details of the antibodies used are shown in Table S1.

Following a previously described protocol (Vaccaro et al., 2020), *in situ* ROS detection was performed by 2',7'-dichlorofluorescein (H2DCF) in fresh E11.5 hearts.

Isolation and culture of primary cardiomyocytes and MEFs

Lonp1$^{F/F}$ and *cTnT-Cre; Lonp1*$^{F/F}$ primary cardiomyocytes were derived from E13.5 hearts. Under aseptic manipulation, each heart was washed in cold PBS three times. The hearts were digested using enzyme buffer (0.1% trypsin and 0.25% collagenase type II) concomitant with shaking at 37 °C in a water bath. Digestion was stopped by adding FBS every ten minutes and pipetting the solution with a pipette. The operation was repeated until no obvious heart tissue was seen. The collected solution was centrifuged, and 1 ml of complete medium was added, followed by transfer to a 6 cm dish. After 2 to 3 hours, nonadherent cardiomyocytes were transferred to new 6 cm dishes. Cultured cardiomyocytes were used to perform IF staining

Lonp1$^{F/F}$ and *ERt2-Cre; Lonp1*$^{F/F}$ MEFs were derived from E13.5 embryos. After removing the head, limbs and internal organs, the remaining tissues were washed with ice-cold PBS, digested with trypsin and cut into pieces. After digestion at 37 ℃ for 15 minutes, the cells were blown to disperse, and then complete medium was added for culture. Then, 0.5 mM 4-OH-tamoxifen (H7904, Sigma–Aldrich) was added for three days to induce Cre expression, and the cells were collected for WB, qPCR and measurement of mtDNA copy number.

Western blot

RIPA buffer (Beyotime Biotechnology, P0013B) with protease inhibitor cocktail (Roche) and PhosSTOP (Roche) was added to ground hearts and PBS washed cells for 30 min. The solution was then centrifuged at 12,000 rpm at 4 °C for 15 minutes. Subsequently, the protein concentration in the collected supernatant was quantified by a BCA Protein Assay Kit (Beyotime, P0012). SDS–PAGE gels (10%) were used to isolate proteins, PVDF membranes (Millipore) were used to transfer proteins, 5% BSA in TBST was used to block proteins, and then PVDF membranes were incubated with different antibodies (Table S1). Because the embryonic heart sample was very small, 2 to 6 hearts were concentrated in a group, and PVDF membranes were cut to incubate different antibodies to save samples. All quantification was performed by ImageJ.

Quantitative real-time PCR

Total RNA was extracted from the cardiac ventricles and different cell lines by using TRIzol reagent (Invitrogen). RNA reverse transcription was performed using a HiScript II Q Select RT Supermix for qPCR (+gDNA wiper) kit (Vazyme Biotech, R223-01). cDNA was used to generate a MicroAmp™ Optical 96-Well Reaction Plate using an AceQ Universal SYBR Master Mix Kit (Vazyme Biotech, Q511-02) and an ABI QuantStudio 5 Real-Time PCR System. Data were processed using the ΔΔCt analytical method with controls normalized to 1 to observe upregulation or downregulation fold. Primers used are detailed in Table S2.

mtDNA copy number assays

We measured the mtDNA copy number of different tissues and cells as previously described (Quiros et al., 2014). Total DNA was extracted using a FastPure DNA Isolation Kit (Vazyme Biotech, DC112-01). RNase was added to ensure no RNA interference. DNA was used in a MicroAmp™ Optical 96-Well Reaction Plate using an AceQ Universal SYBR Master Mix Kit (Vazyme Biotech, Q511-02) and an ABI QuantStudio 5 Real-Time PCR System. Primers used are detailed in Table S2.

Cell culture and treatment assays

Adherent cells were cultured in complete medium (high-glucose DMEM, 12800017, Gibco™) supplemented with 10% fetal bovine serum (FSP500, Excell Bio) and 100 U/ml penicillin–streptomycin (15140122, Gibco™) at 37 °C and 5% CO_2.

For RNAi, a small interfering RNA (*siRNA*) duplex, shown below, was designed to knockdown *Lonp1*. *siLonp1*-1: sense, 5′-GGGACAUCAUUGCCUUGAATT-3′; antisense, 5′-UUCAAG-GCAAUGAUGUCCCTT-3′; *siLonp1*-2: sense, 5′-CCGAGAACAAGAAGGACUUTT-3′; antisense, 5′-AAGUCCUUCUUGUUCUCGGTT-3′. Mixed *siLonp1* was used to treat cells to achieve higher knockdown efficiency. According to the protocol, transfection was performed using GP-Transfect mate (GenePharma). Cells were harvested for WB and qPCR analysis.

For overexpression, different plasmids were constructed and transfected into 293T cells using Lipo2000 (Invitrogen) according to the manufacturer's protocol. Primers used are detailed in Table S3. Cells were collected for WB, qPCR and measurement of mtDNA copy number. For CDDO treatment, cells normally cultured to 80% density were supplemented with CDDO. The concentration of CDDO and the time of treatment

varied depending on the experimental requirements. Cells were harvested for WB and qPCR analysis.

Luciferase reporter assays

The full-length fragment of the mouse ATF4 coding sequence (CDS) was cloned into the pCMV7.1-3×FLAG vector. Based on the results predicted by the website (https://jaspar.genereg.net/), we cloned the ~2 kb *Glut1* promoter fragment and an ~2 kb *Tfam* promoter fragment into the pGL3-Basic Vector (Promega) to generate the *Glut1*-2K Luc vector and *Tfam*-2K Luc vector, respectively. Primers used are detailed in Table S3. Plasmids were transfected into cells using Lipo2000 (Invitrogen). Luciferase reporter assays in 293T cells were performed using the Dual Luciferase Assay System (Promega) by following a standard protocol after 24-36 h of transfection.

Statistical analysis

All experimental statistics and quantitative results are reported as the means, and the error bars represent the s.e.m. by using GraphPad Prism 8.0 software. Differences between mean values were compared by two-tailed unpaired Student's *t* test or one-way ANOVA and two-way ANOVA. We defined $p < 0.05$ (*) as a significant difference.

Acknowledgements

We thank Dr. Bin Zhou (Albert Einstein College of Medicine, New York) for providing the *cTnT-Cre* mice.

Conflicts of interest

The authors declare that they have no competing interests.

Author contributions

Conceptualization: K. Z., Z. Y. Methodology: K. Z., X. H. and W. Z. Resource: B. L. Investigation: K. Z. X. H. Supervision: Z. Y. Writing – original draft: K. Z. Writing – review & editing: K. Z. and Z. Y.

Funding and additional information

This work was supported by grants from the National Key Research and Development Program of China (2019YFA0801601) and grants from the National Natural Science Foundation of China (31930029, 91854111, 91954101 and 31771534) to Zhongzhou Yang and Bin Lu.

Data availability

All data are available in the main text or the supplementary materials. RNA-seq data has been uploaded to the SRA database with the accession number PRJNA800234.

REFERENCES

B'Chir, W., Maurin, A. C., Carraro, V., Averous, J., Jousse, C., Muranishi, Y., Parry, L., Stepien, G., Fafournoux, P. and Bruhat, A. (2013) 'The eIF2α/ATF4 pathway is essential for stress-induced autophagy gene expression', *Nucleic Acids Res* **41**(16): 7683-99.

Bernstein, S. H., Venkatesh, S., Li, M., Lee, J., Lu, B., Hilchey, S. P., Morse, K. M., Metcalfe, H. M., Skalska, J., Andreeff, M. et al. (2012) 'The mitochondrial ATP-dependent Lon protease: a novel target in lymphoma death mediated by the synthetic triterpenoid CDDO and its derivatives', *Blood* **119**(14): 3321-9.

Bruneau, B. G. (2020) 'The developing heart: from The Wizard of Oz to congenital heart disease', *Development* **147**(21).

Chen, S. H., Suzuki, C. K. and Wu, S. H. (2008) 'Thermodynamic characterization of specific interactions between the human Lon protease and G-quartet DNA', *Nucleic Acids Res* **36**(4): 1273-87.

Dara, L., Ji, C. and Kaplowitz, N. (2011) 'The contribution of endoplasmic reticulum stress to liver diseases', *Hepatology* **53**(5): 1752-63.

Fischer, F., Hamann, A. and Osiewacz, H. D. (2012) 'Mitochondrial quality control: an integrated network of pathways', *Trends Biochem Sci* **37**(7): 284-92.
Guimarães-Camboa, N., Stowe, J., Aneas, I., Sakabe, N., Cattaneo, P., Henderson, L., Kilberg, M. S., Johnson, R. S., Chen, J., McCulloch, A. D. et al. (2015) 'HIF1α Represses Cell Stress Pathways to Allow Proliferation of Hypoxic Fetal Cardiomyocytes', *Dev Cell* **33**(5): 507-21.
Harvey, R. P. (2002) 'Patterning the vertebrate heart', *Nat Rev Genet* **3**(7): 544-56.
Jousse, C., Oyadomari, S., Novoa, I., Lu, P., Zhang, Y., Harding, H. P. and Ron, D. (2003) 'Inhibition of a constitutive translation initiation factor 2alpha phosphatase, CReP, promotes survival of stressed cells', *J Cell Biol* **163**(4): 767-75.
Kao, T. Y., Chiu, Y. C., Fang, W. C., Cheng, C. W., Kuo, C. Y., Juan, H. F., Wu, S. H. and Lee, A. Y. (2015) 'Mitochondrial Lon regulates apoptosis through the association with Hsp60-mtHsp70 complex', *Cell Death Dis* **6**(2): e1642.
Kilberg, M. S., Shan, J. and Su, N. (2009) 'ATF4-dependent transcription mediates signaling of amino acid limitation', *Trends Endocrinol Metab* **20**(9): 436-43.
Koyanagi, S., Hamdan, A. M., Horiguchi, M., Kusunose, N., Okamoto, A., Matsunaga, N. and Ohdo, S. (2011) 'cAMP-response element (CRE)-mediated transcription by activating transcription factor-4 (ATF4) is essential for circadian expression of the Period2 gene', *J Biol Chem* **286**(37): 32416-23.
Lopaschuk, G. D. and Jaswal, J. S. (2010) 'Energy metabolic phenotype of the cardiomyocyte during development, differentiation, and postnatal maturation', *J Cardiovasc Pharmacol* **56**(2): 130-40.
Lu, B., Lee, J., Nie, X., Li, M., Morozov, Y. I., Venkatesh, S., Bogenhagen, D. F., Temiakov, D. and Suzuki, C. K. (2013) 'Phosphorylation of human TFAM in mitochondria impairs DNA binding and promotes degradation by the AAA+ Lon protease', *Mol Cell* **49**(1): 121-32.
Lu, P. D., Harding, H. P. and Ron, D. (2004) 'Translation reinitiation at alternative open reading frames regulates gene expression in an integrated stress response', *J Cell Biol* **167**(1): 27-33.
Maroli, G. and Braun, T. (2021) 'The long and winding road of cardiomyocyte maturation', *Cardiovasc Res* **117**(3): 712-726.
Matsushima, Y., Goto, Y. and Kaguni, L. S. (2010) 'Mitochondrial Lon protease regulates mitochondrial DNA copy number and transcription by selective degradation of mitochondrial transcription factor A (TFAM)', *Proc Natl Acad Sci U S A* **107**(43): 18410-5.
Menendez-Montes, I., Escobar, B., Palacios, B., Gómez, M. J., Izquierdo-Garcia, J. L., Flores, L., Jiménez-Borreguero, L. J., Aragones, J., Ruiz-Cabello, J., Torres, M. et al. (2016) 'Myocardial VHL-HIF Signaling Controls an Embryonic Metabolic Switch Essential for Cardiac Maturation', *Dev Cell* **39**(6): 724-739.
Olson, E. N. and Srivastava, D. (1996) 'Molecular pathways controlling heart development', *Science* **272**(5262): 671-6.
Pakos-Zebrucka, K., Koryga, I., Mnich, K., Ljujic, M., Samali, A. and Gorman, A. M. (2016) 'The integrated stress response', *EMBO Rep* **17**(10): 1374-1395.
Quiros, P. M., Espanol, Y., Acin-Perez, R., Rodriguez, F., Barcena, C., Watanabe, K., Calvo, E., Loureiro, M., Fernandez-Garcia, M. S., Fueyo, A. et al. (2014) 'ATP-dependent Lon protease controls tumor bioenergetics by reprogramming mitochondrial activity', *Cell Rep* **8**(2): 542-56.
Quirós, P. M., Prado, M. A., Zamboni, N., D'Amico, D., Williams, R. W., Finley, D., Gygi, S. P. and Auwerx, J. (2017) 'Multi-omics analysis identifies ATF4 as a key regulator of the mitochondrial stress response in mammals', *J Cell Biol* **216**(7): 2027-2045.
Rugarli, E. I. and Langer, T. (2012) 'Mitochondrial quality control: a matter of life and death for neurons', *Embo j* **31**(6): 1336-49.
Shin, C. S., Meng, S., Garbis, S. D., Moradian, A., Taylor, R. W., Sweredoski, M. J., Lomenick, B. and Chan, D. C. (2021) 'LONP1 and mtHSP70 cooperate to promote mitochondrial protein folding', *Nat Commun* **12**(1): 265.
Song, J., Herrmann, J. M. and Becker, T. (2021) 'Quality control of the mitochondrial proteome', *Nat Rev Mol Cell Biol* **22**(1): 54-70.
Suzuki, C. K., Suda, K., Wang, N. and Schatz, G. (1994) 'Requirement for the yeast gene LON in intramitochondrial proteolysis and maintenance of respiration', *Science* **264**(5156): 273-6.
Vaccaro, A., Kaplan Dor, Y., Nambara, K., Pollina, E. A., Lin, C., Greenberg, M. E. and Rogulja, D. (2020) 'Sleep Loss Can Cause Death through Accumulation of Reactive Oxygen Species in the Gut', *Cell* **181**(6): 1307-1328.e15.
Vattem, K. M. and Wek, R. C. (2004) 'Reinitiation involving upstream ORFs regulates ATF4 mRNA translation in mammalian cells', *Proc Natl Acad Sci U S A* **101**(31): 11269-74.

Xu, M., Yao, J., Shi, Y., Yi, H., Zhao, W., Lin, X. and Yang, Z. (2021) 'The SRCAP chromatin remodeling complex promotes oxidative metabolism during prenatal heart development', *Development* **148**(8).
Zhao, Q., Sun, Q., Zhou, L., Liu, K. and Jiao, K. (2019) 'Complex Regulation of Mitochondrial Function During Cardiac Development', *J Am Heart Assoc* **8**(13): e012731.
Zurita Rendon, O. and Shoubridge, E. A. (2018) 'LONP1 Is Required for Maturation of a Subset of Mitochondrial Proteins, and Its Loss Elicits an Integrated Stress Response', *Mol Cell Biol* **38**(20).

Figures

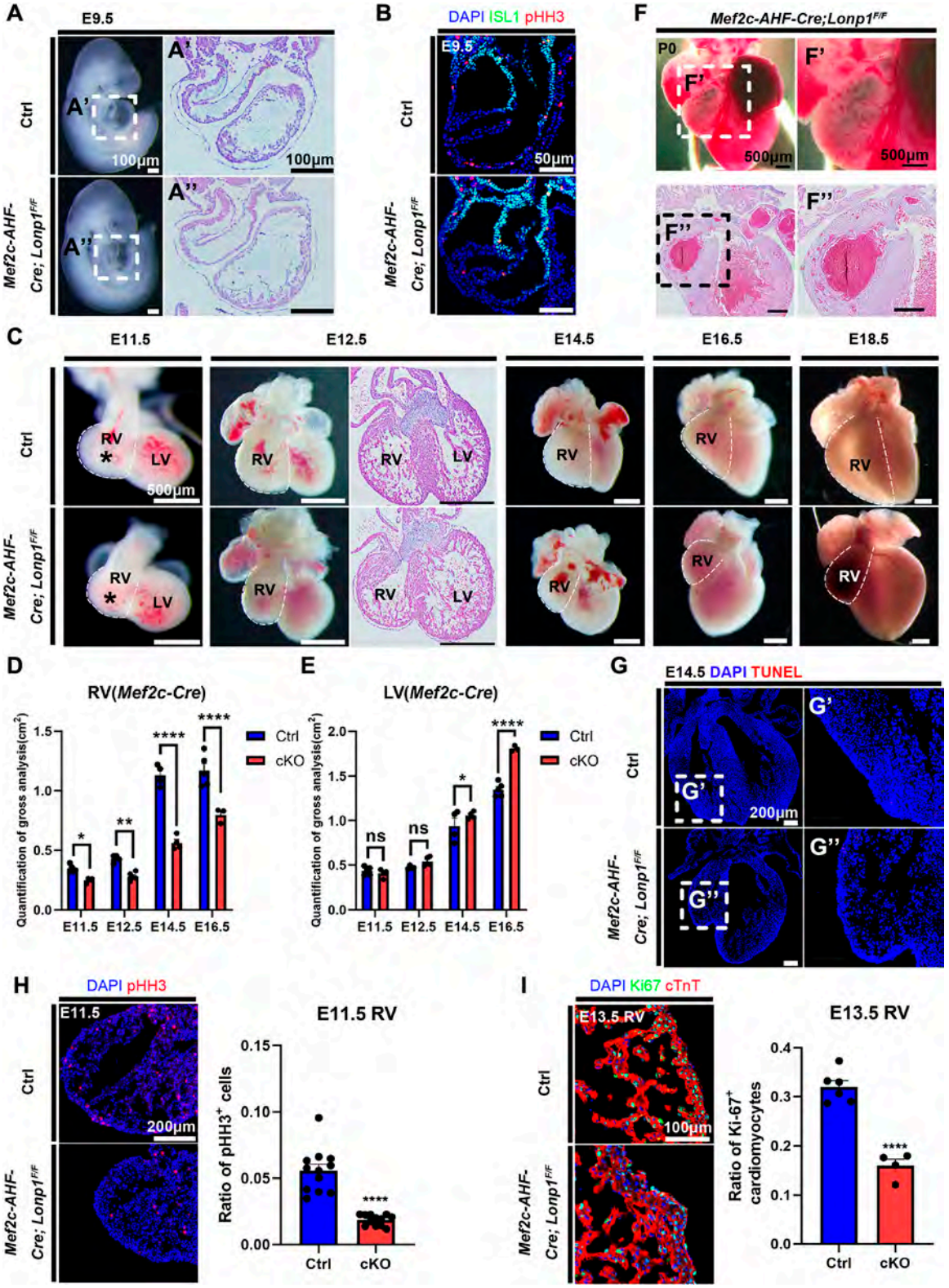

Fig. 1. Deletion of *Lonp1* in cardiac progenitors caused right ventricular hypoplasia. (**A**) Gross analysis of embryos and hematoxylin and eosin (H&E) staining of heart tissues at E9.5 (n=5). Right panels (**A'** and **A''**) were H&E staining. (**B**) Cell proliferation and $ISL1^+$ progenitor cell distribution (n=3). (**C**) Gross analysis of hearts at different embryonic stages and H&E staining of hearts at E12.5 (n=3-5). An asterisk indicates a reduction in RV volume starting at E11.5. The dotted line outlines the right ventricle. RV, right ventricle; LV, left ventricle. (**D, E**) Quantification of RV (**D**) and LV (**E**) areas of (**C**) (n=3-5). (**F**) Gross analysis and H&E staining of *Lonp1*-deficient hearts at P0. Right panels showed higher magnification of dashed box. (**G**) TUNEL staining of the two ventricles at E14.5. Right panels show higher magnification of dashed box. (**H**) Cell proliferation analysis and quantification of the RV at E11.5 (n=12). (**I**) Cardiomyocyte proliferation analysis and quantification of RV at E13.5 (n=6 vs 4). CM marker: cTnT. Data are mean±s.e.m. **p* <0.05, ***p* <0.01, *****p* <0.0001 (two-tailed unpaired Student's *t* test). ns, not significant.

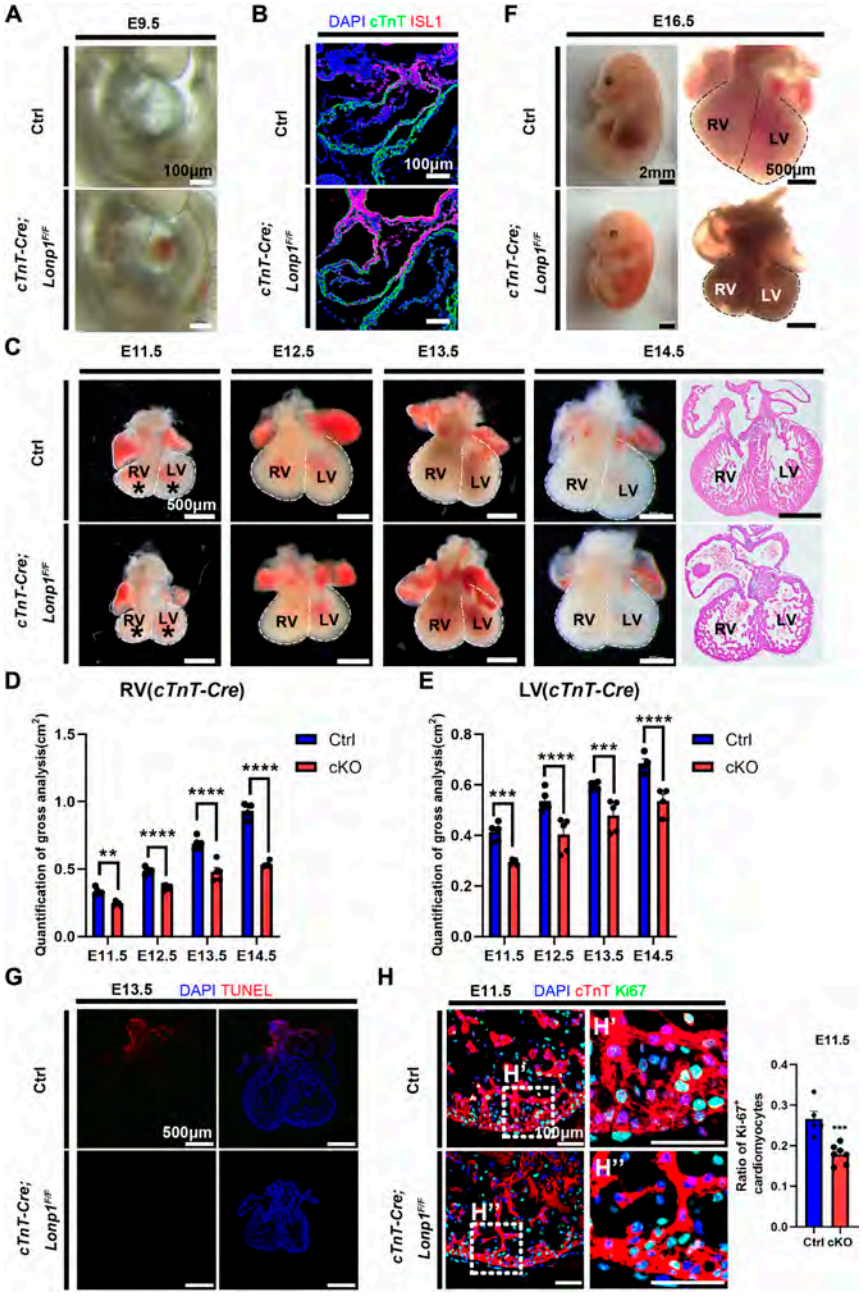

Fig. 2. *Lonp1* deficiency in embryonic cardiomyocytes impaired myocardial development. (**A**) Gross analysis of embryos at E9.5 (n=3). (**B**) ISL1^{+} progenitor cell distribution. (**C**) Gross analysis of hearts at different embryonic stages and H&E staining of heart tissues at E14.5. The asterisks indicate a reduction in ventricular volume starting at E11.5. The dotted line outlines the two ventricles. (**D, E**) Quantification of RV (**D**) and LV (**E**) areas of (**C**) (n=4-5). (**F**) Gross analysis of embryos and hearts at E16.5. The dotted line outlines the two ventricles. All *Lonp1* mutant embryos died after E16.5 (n=4-6). (**G**) TUNEL staining of the ventricles at E13.5. (**H**) Cell proliferation analysis of cardiomyocytes and quantification at E11.5 (n=5 vs 7). Right panels show higher magnification of (**H'** and **H''**) in the left panels. Data are mean±s.e.m. ***p* <0.01, ****p* <0.001, *****p* <0.0001 (two-tailed unpaired Student's *t* test).

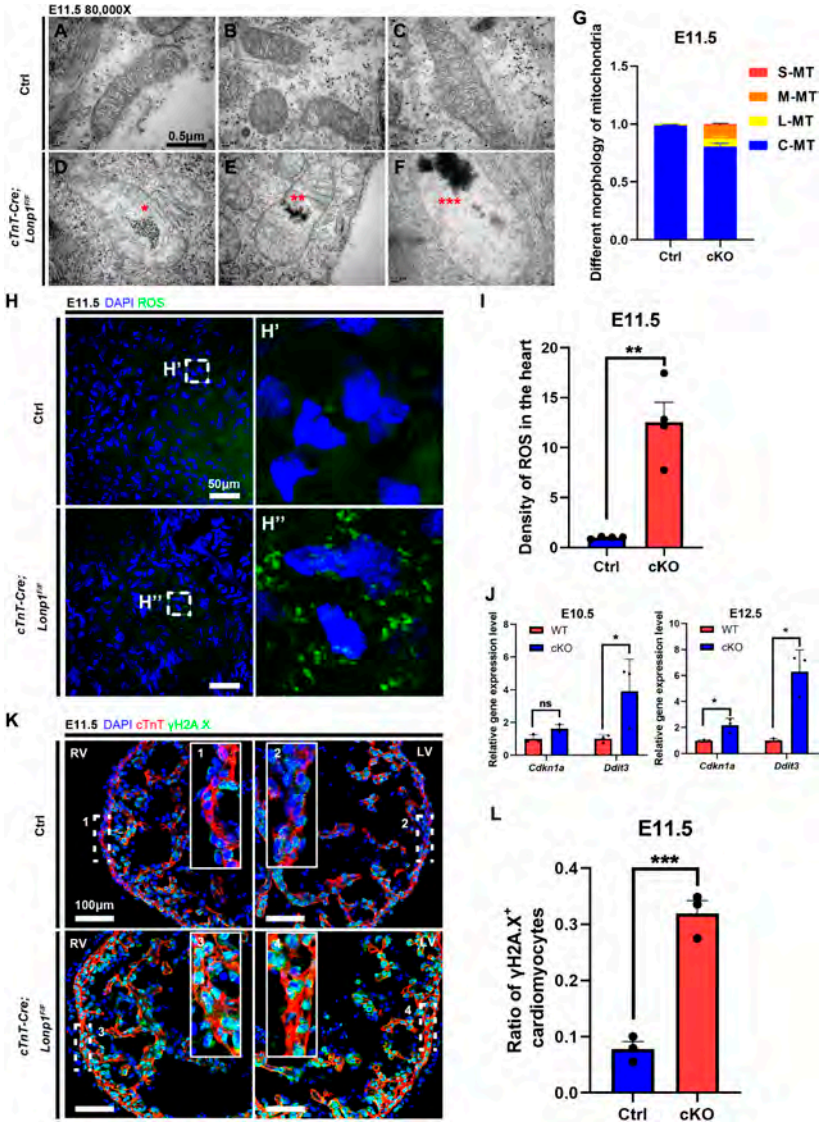

Fig. 3. *Lonp1* deficiency caused mitochondrial abnormalities, increased ROS production and DNA damage. (**A-F**) Transmission electron microscopy (TEM) images show the mitochondria in the cardiomyocytes at E11.5. Control groups (**A-C**) have normal mitochondria. *Lonp1* depletion groups (**D-F**) show accumulation of aggregates, mitochondrial swelling and disappearance of mitochondrial cristae (red asterisk). (**G**) Quantification of different morphology of mitochondria. C-MT means completed mitochondria; L-MT means lightly damaged mitochondria as represented in (**D**); M-MT means moderately damaged mitochondria as represented in (**E**); S-MT means severely damaged mitochondria as represented in (**F**) (n=3). cKO is *cTnT-Cre; Lonp1* $^{F/F}$. (**H**) Oxidized H2DCF (green) represents an increase in ROS levels in the hearts of *Lonp1* deficiency mice. Right panels show higher magnification of dashed box. (**I**) Quantification of density of ROS in the heart (n=4). (**J**)Expression level of genes associated with cell cycle inhibition in E10.5 and E12.5 hearts (n=3). (**K**) IF staining shows increased level of γH2A. X, a DNA damage marker in *Lonp1* mutant cardiomyocytes (n=3). Numbered panels show higher magnification of dashed box. LV, left ventricle; RV, right ventricle. (**L**) Quantification of (**K**). Data are mean±s.e.m. **p* <0.05, ***p* <0.01, ****p* <0.001 (two-tailed unpaired Student's *t* test). ns, not significant.

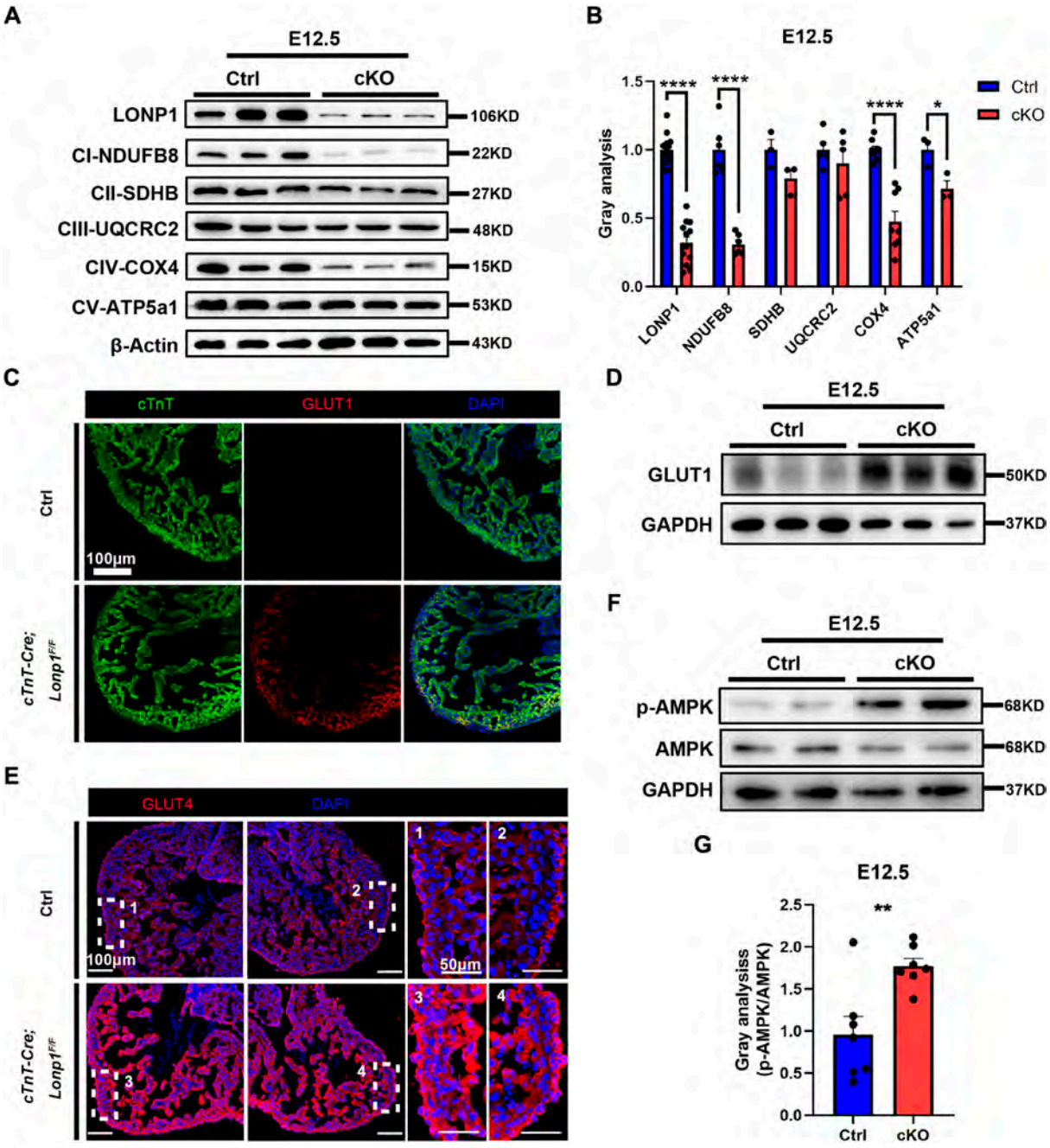

Fig. 4. Altered metabolic pattern in *Lonp1* mutant heart. (**A, B**) Western blot analysis (**A**) and quantification (**B**) of components of respiratory chain complexes in E12.5 hearts (n=3-12). cKO is *cTnT-Cre; Lonp1*$^{F/F}$. (**C**) IF staining shows increased GLUT1 levels in ventricles (n=3). (**D**) Western blot analysis of GLUT1 in E12.5 hearts (n=6). (**E**) IF staining shows increased GLUT4 levels in ventricles (n=3). Right panels show higher magnification of dashed box. (**F, G**) Western blot analysis (**F**) and quantification (**G**) of p-AMPK in E12.5 hearts (n=7). Data are mean±s.e.m. **p* <0.05, ***p* <0.01, *****p* <0.0001 (two-tailed unpaired Student's *t* test).

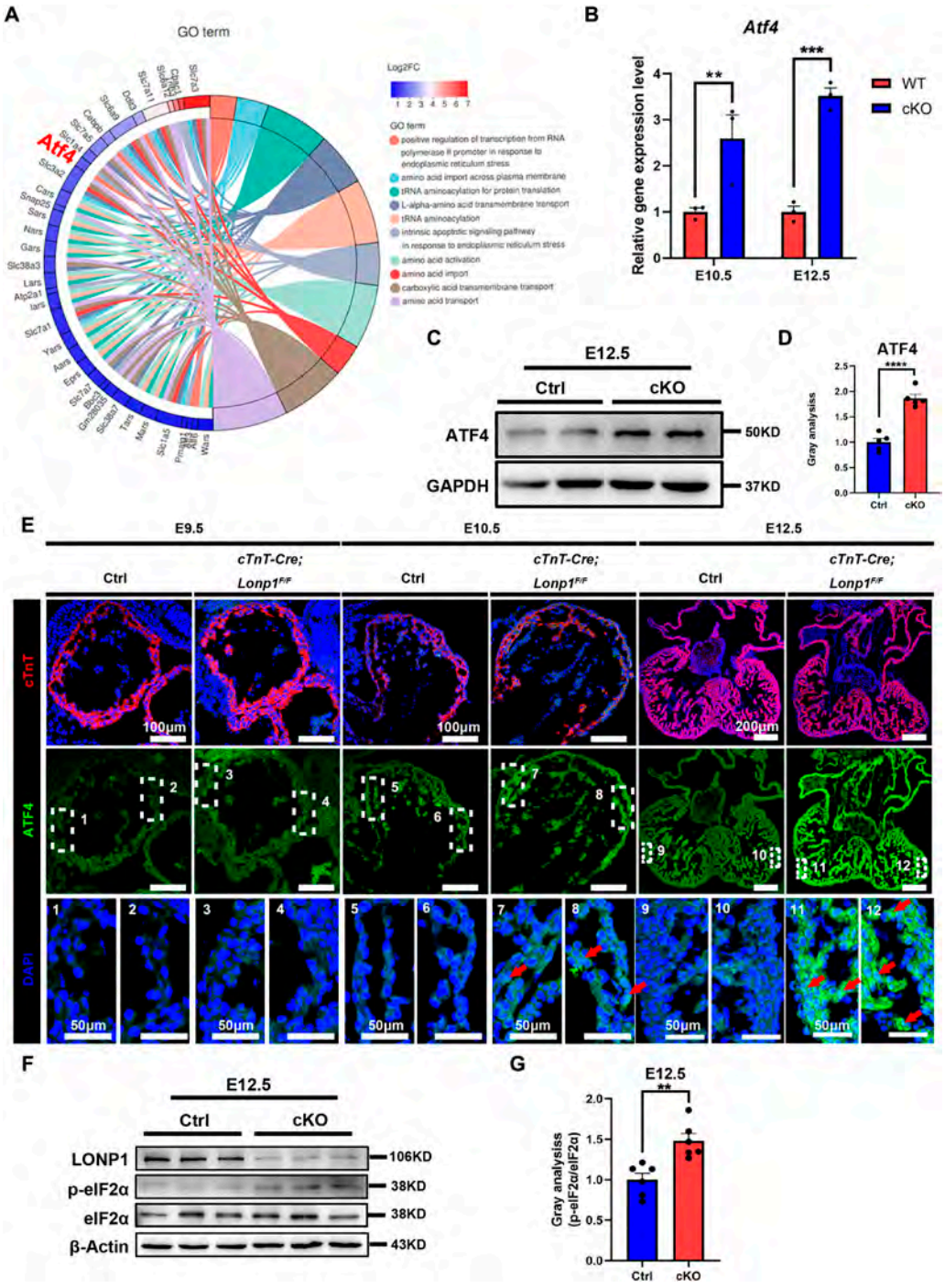

Fig. 5. Enhanced ATF4 level in *Lonp1* mutant hearts. (**A**) Comprehensive alignment of the altered genes (left) and Gene Ontology (GO) analysis (right). ATF4 is highlighted. (**B**) Expression of *Atf4* in E10.5 and E12.5 hearts (n=3). cKO is *cTnT-Cre; Lonp1*$^{F/F}$. (**C, D**) Western blot analysis (**C**) and quantification (**D**) of ATF4 in E12.5 hearts (n=5). (**E**) IF staining shows that the level of ATF4 gradually increases with cardiac development in *Lonp1* deficiency. The red arrow indicates ATF4 colocated with DAPI. Bottom panels show higher magnification of dashed box (n=3). (**F, G**) Western blot analysis (**F**) and quantification (**G**) of p-eIF2α in E12.5 hearts (n=6). Data are mean±s.e.m. ***p* <0.01, *** *p* <0.001, **** *p* <0.0001 (two-tailed unpaired Student's *t* test).

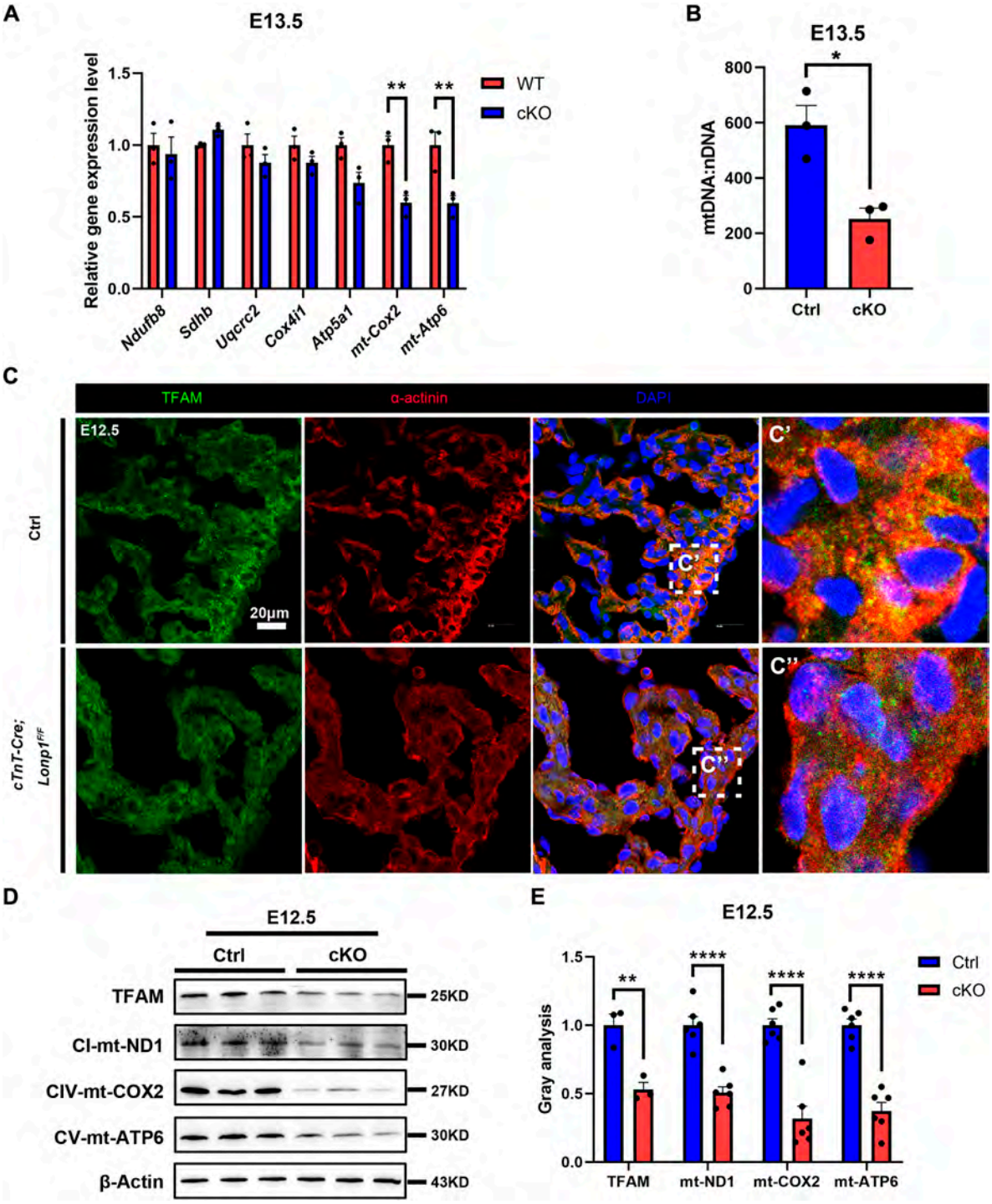

Fig. 6. *Lonp1* deficiency reduced the levels of TFAM, mtDNA and mtDNA-encoded respiratory chain complex components. (**A**) Expression of nuclear DNA and mtDNA genes encoding respiratory chain complex components in E13.5 hearts. cKO is *cTnT-Cre; Lonp1*$^{F/F}$ (n=3). (**B**) mtDNA copy number in E13.5 hearts (n=3). (**C**) IF staining shows a decrease in TFAM levels in *Lonp1* mutant hearts (n=3). Right panels show higher magnification of dashed box. (**D, E**) Western blot analysis (**D**) and quantification (**E**) of TFAM- and mtDNA-encoded respiratory chain complex components in E12.5 hearts (n=3-6). Data are mean±s.e.m. *p <0.05, ** p <0.01, **** p <0.0001 (two-tailed unpaired Student's t test).

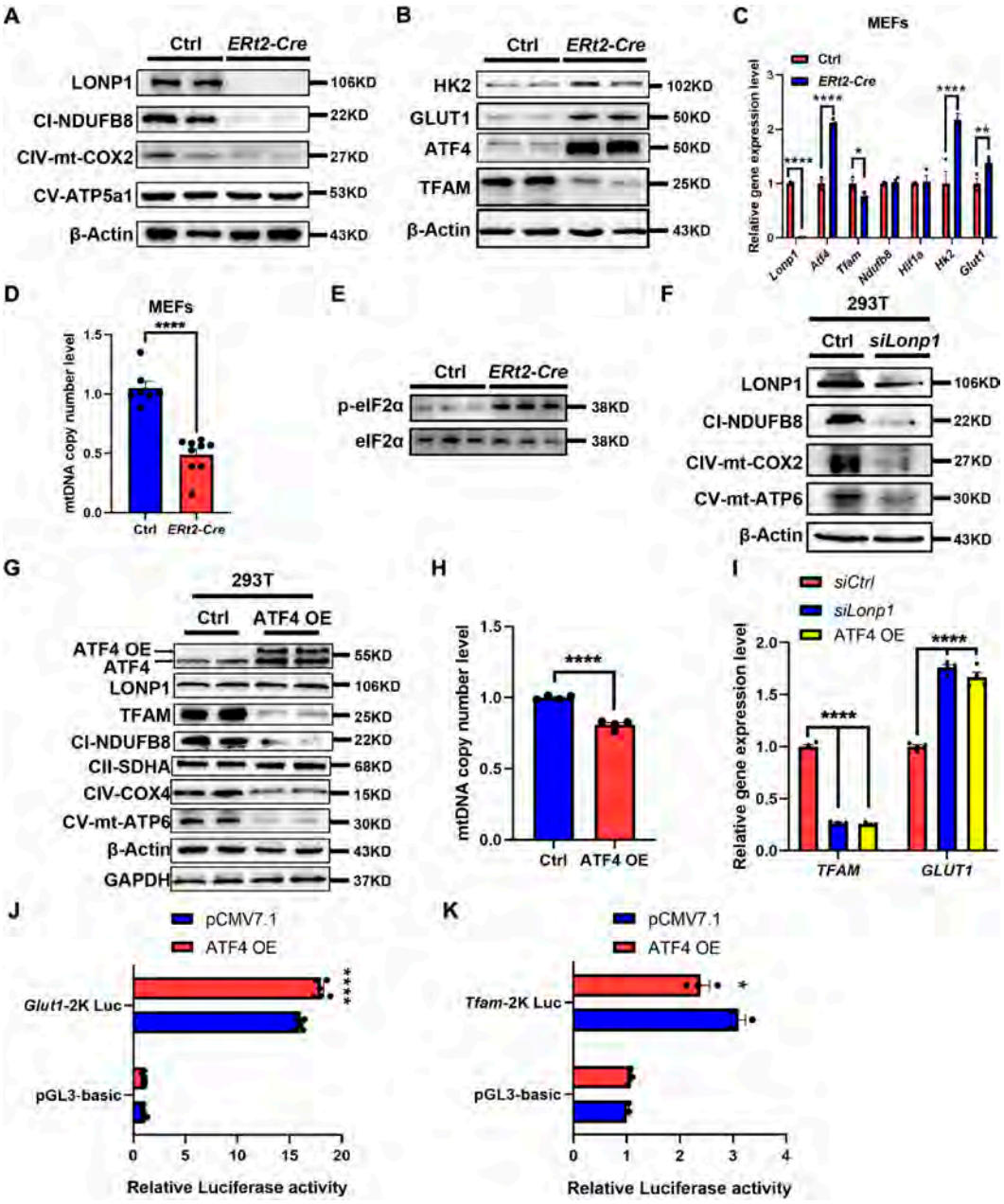

Fig. 7. ATF4 directly regulated *Tfam* and *Glut1* transcription. (**A**) Western blot analysis of respiratory chain complex components in MEFs. *ERt2-Cre* is *ERt2-Cre; Lonp1*$^{F/F}$+4-OH Tamoxifen (n=3-6). (**B**) Western blot analysis in MEFs (n=3-6). (**C**) Gene expression study in MEFs (n=3). (**D**) mtDNA copy number in MEFs (n=7 vs 9). (**E**) Western blot analysis of p-eIF2α in MEFs (n=3). (**F**) Western blot analysis of respiratory chain complex components in 293T cells (n=3-6). *siLonp1* means *Lonp1* knockdown. (**G**) Western blot analysis in 293T cells (n=5-6). ATF4 OE means ATF4 overexpression. (**H**) mtDNA copy number in 293T cells (n=4). (**I**) Expression of *Tfam* and *Glut1* in *siLonp1*- and ATF4-OE 293T cells (n=4). **(J, K)** The luciferase reporter assay revealed that ATF4 can activate the promoter activity of *Glut1* (**J**) but repress the promoter activity of *Tfam* (**K**) (n=6 and 3). Data are mean±s.e.m. **p* <0.05, **P<0.01, **** *p* <0.0001 (two-tailed unpaired Student's *t* test or two-way ANOVA).

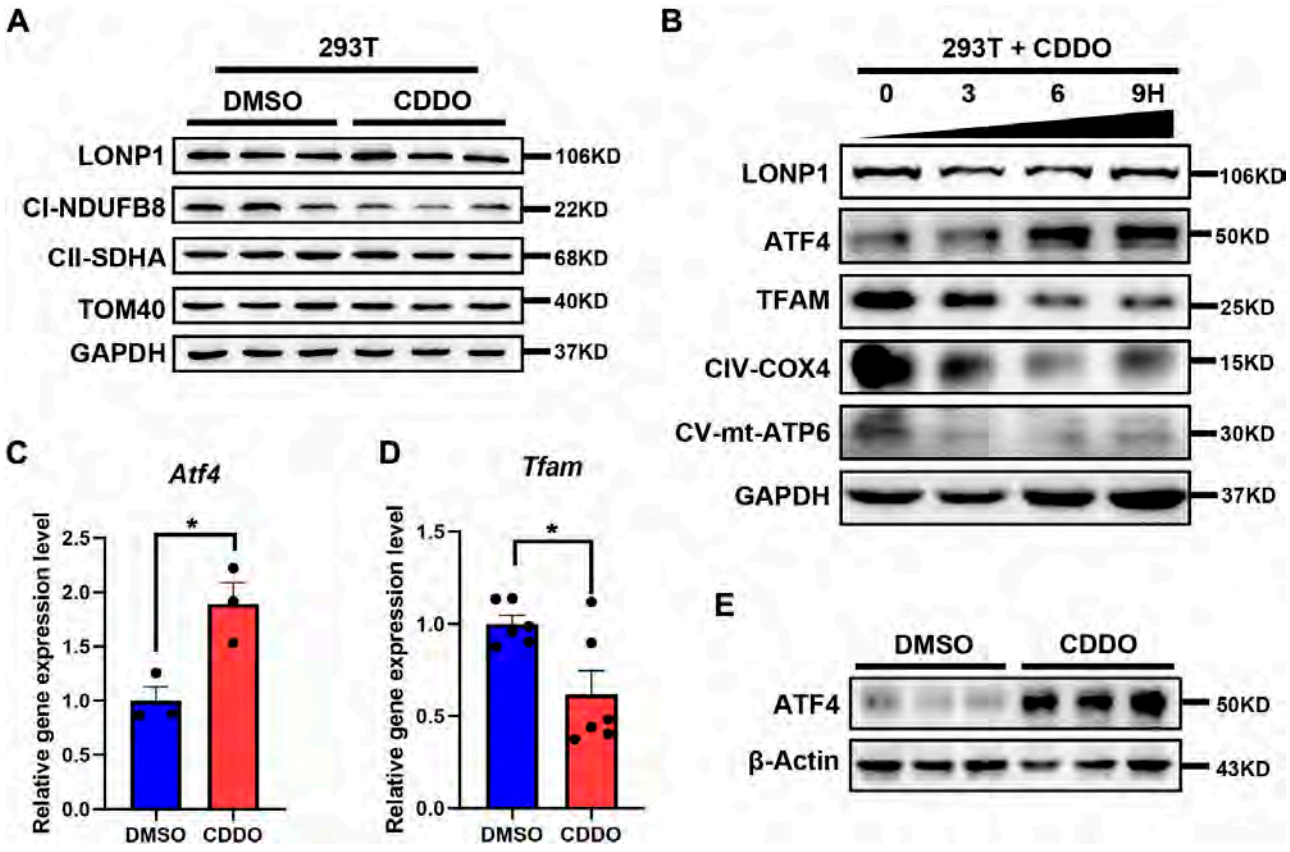

Fig. 8. CDDO treatment mimicked *Lonp1* deficiency. (**A**) Western blot analysis of respiratory chain complex components in 293T cells treated with 2.5 μM CDDO for 10 hours (n=3). (**B**) Western blot analysis in 293T cells treated with 2.5 μM CDDO (n=3). (**C, D**) Expression of *Atf4* (**C**) and *Tfam* (**D**) in 293T cells treated with 2.5 μM CDDO (10 hours, n=3 and 6). (**E**) Western blot analysis of ATF4 using the same materials as in (**C**) (n=3). Data are mean±s.e.m. **p* <0.05 (two-tailed unpaired Student's *t* test).

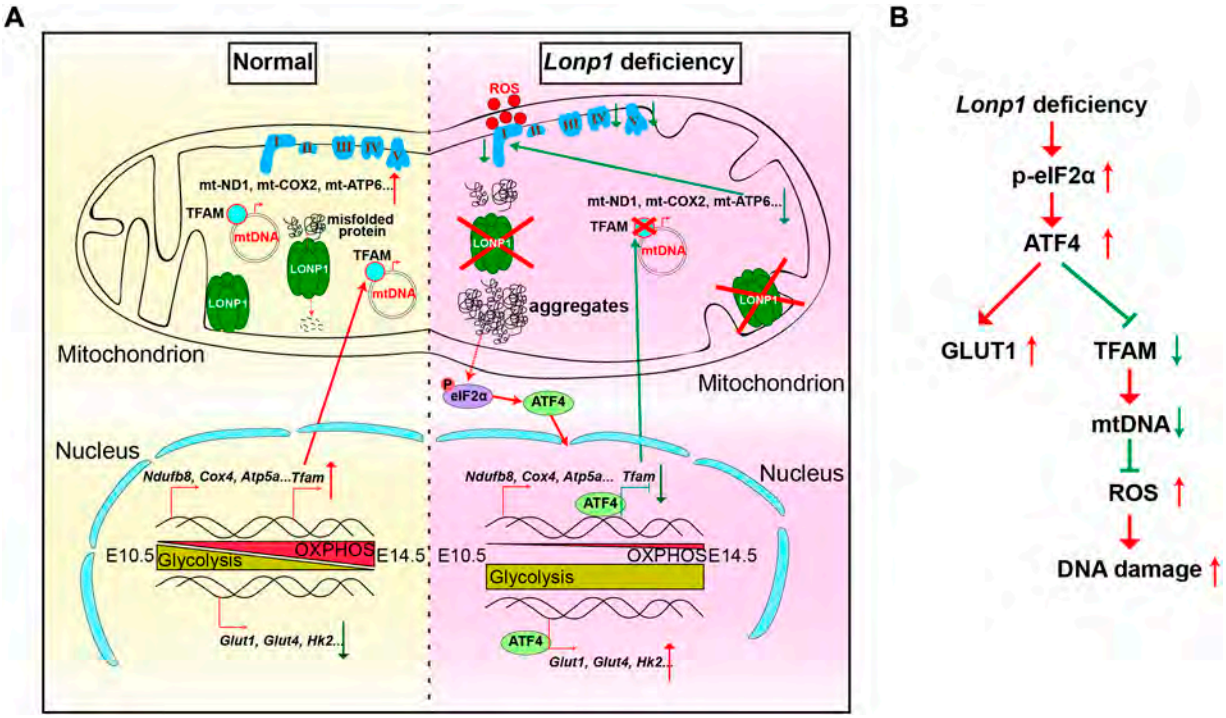

Fig. 9. Working model. (**A**) Under normal conditions (left), a metabolic shift from anaerobic glycolysis to oxidative phosphorylation takes place at approximately E10.5. LONP1 degrades misfolded or oxidized proteins to safeguard the metabolic shift and cardiac development. In the absence of *Lonp1* (right), misfolded or oxidized proteins formed aggregates, which activated the p-eIF2α-ATF4 signaling pathway. Subsequently, ATF4 promoted *Glut1* expression but repressed *Tfam* expression by directly binding to their promoters. Decreased TFAM levels reduced the amount and transcription of mtDNA, and the assembly of respiratory chain complexes was greatly affected. Mitochondrial dysfunction generates a large amount of ROS, which causes DNA damage and inhibits cell proliferation. In panel (**B**), the red arrows indicate advancement, and the green arrows indicate inhibition.

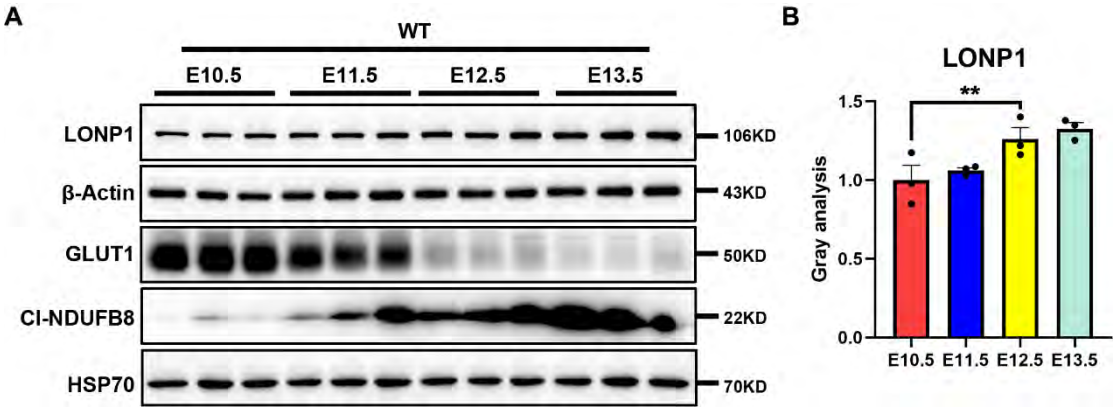

Fig. S1. Western blot analysis and quantitative analysis. (**A**) Western blot analysis of embryonic heart tissues (n=3). (**B**) Quantification of LONP1. Data are mean ±s.e.m. $^{**}p<0.01$ (one-way ANOVA).

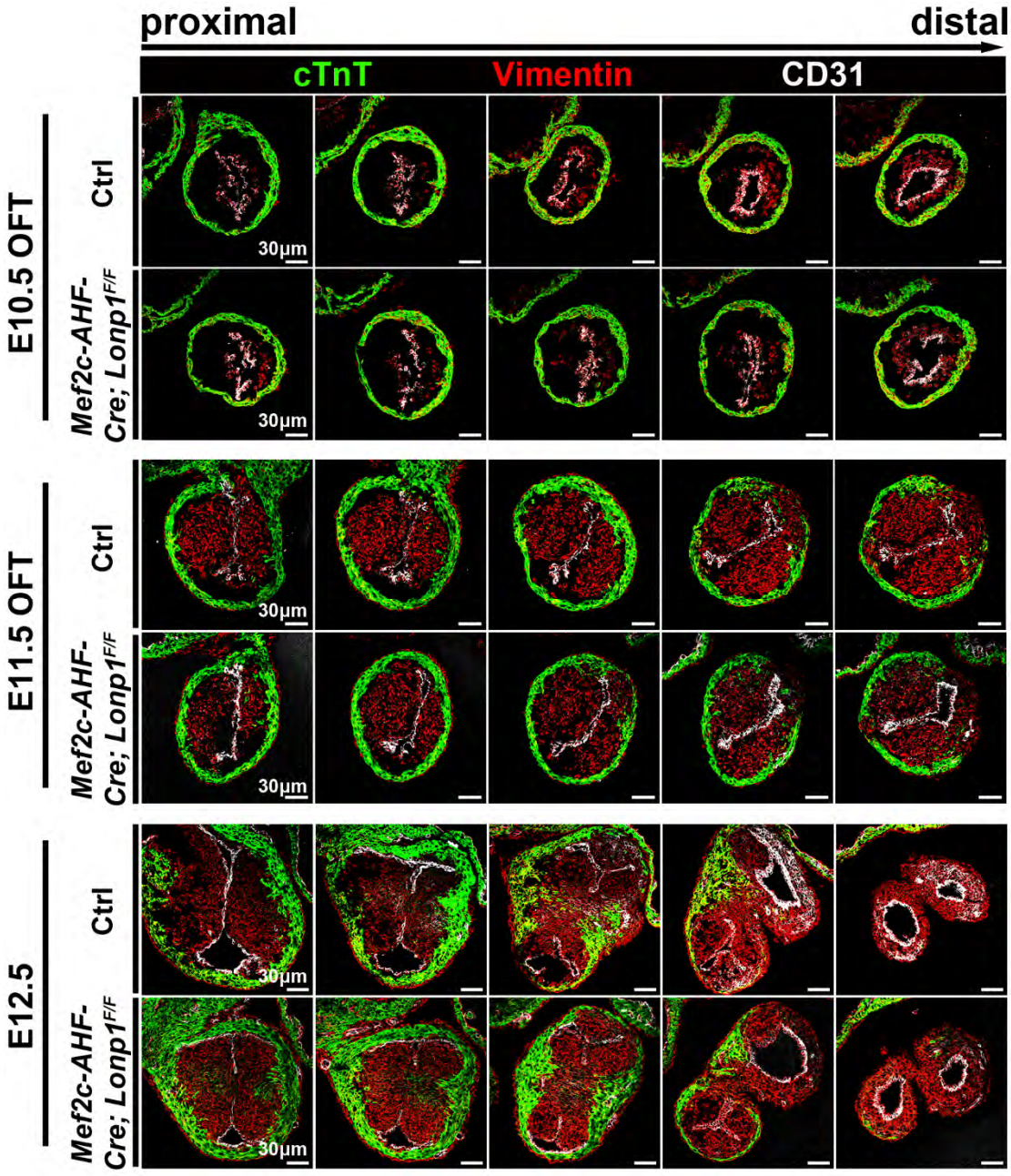

Fig. S2. Deletion of *Lonp1* in cardiac progenitors did not affect OFT morphogenesis and septation. IF staining showed normal OFT morphology and septation in the absence of LONP1 (n=3). Mesenchymal cell marker: Vimentin; endothelial cell marker: CD31.

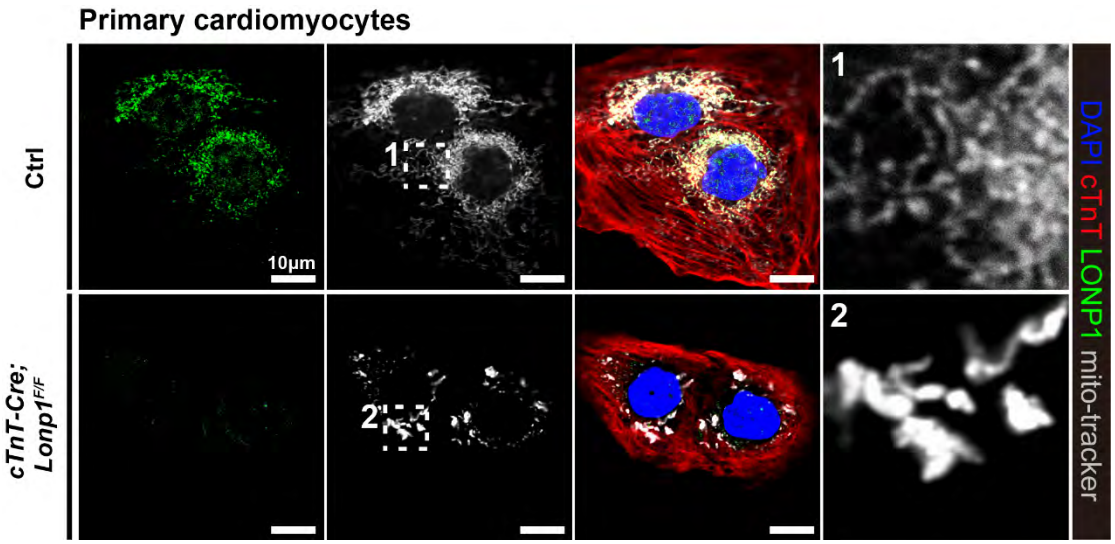

Fig. S3. Morphological changes in mitochondria in *Lonp1*-deficient cardiomyocytes. IF staining showed the morphology of mitochondria in cardiomyocytes. Right panels show higher magnification of dashed boxes. Mitochondria marker: mito-tracker.

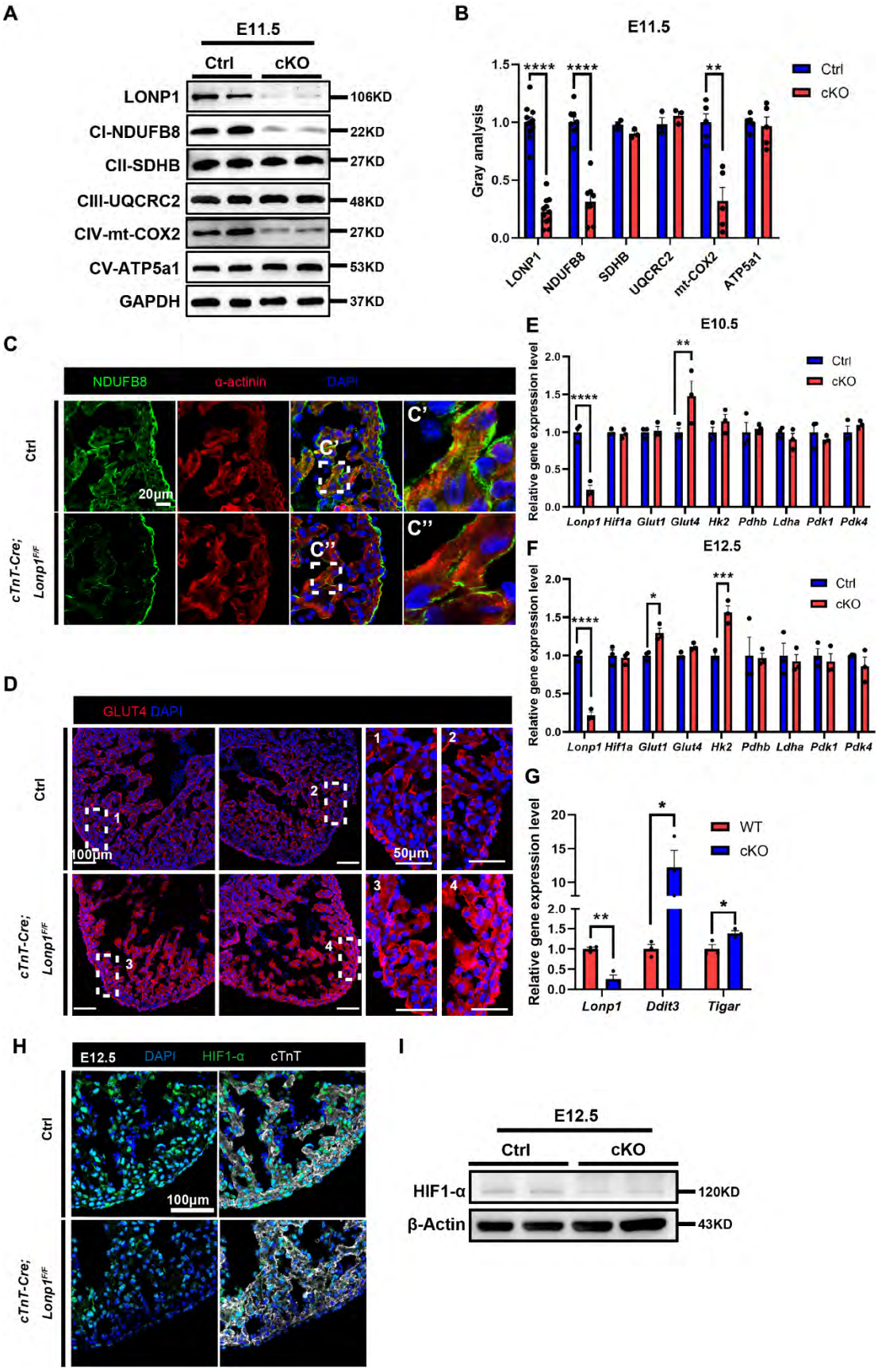

Fig. S4. LONP1 maintained the metabolic shift of cardiac development. (**A, B**) Western blot analysis (**A**) and quantification (**B**) of respiratory chain complexes in E11.5 hearts (n=3-11). (**C**) IF staining shows a decrease in mitochondria localized between sarcomeres in the hearts of *Lonp1*

deficiency (n=3). Right panels show higher magnification of dashed box. CM marker: α-actinin. (**D**) IF staining shows increased GLUT4 levels in ventricles (n=3). Right panels show higher magnification of dashed box. (**E, F**) Expression of glycolysis-related genes in E10.5 (**E**) and E12.5 (**F**) hearts (n=3). (**G**) Expression of *Tigar*, which inhibits glycolysis-related gene transcription (n=3). (**H**) IF staining shows decreased protein level of HIF1-α in cardiomyocyte at E12.5. (**I**) Western blot analysis of HIF1-α in E12.5 hearts. Data are mean±s.e.m. *p<0.05, **p<0.01, ***p<0.001, ****p<0.0001 (two-tailed unpaired Student's t test).

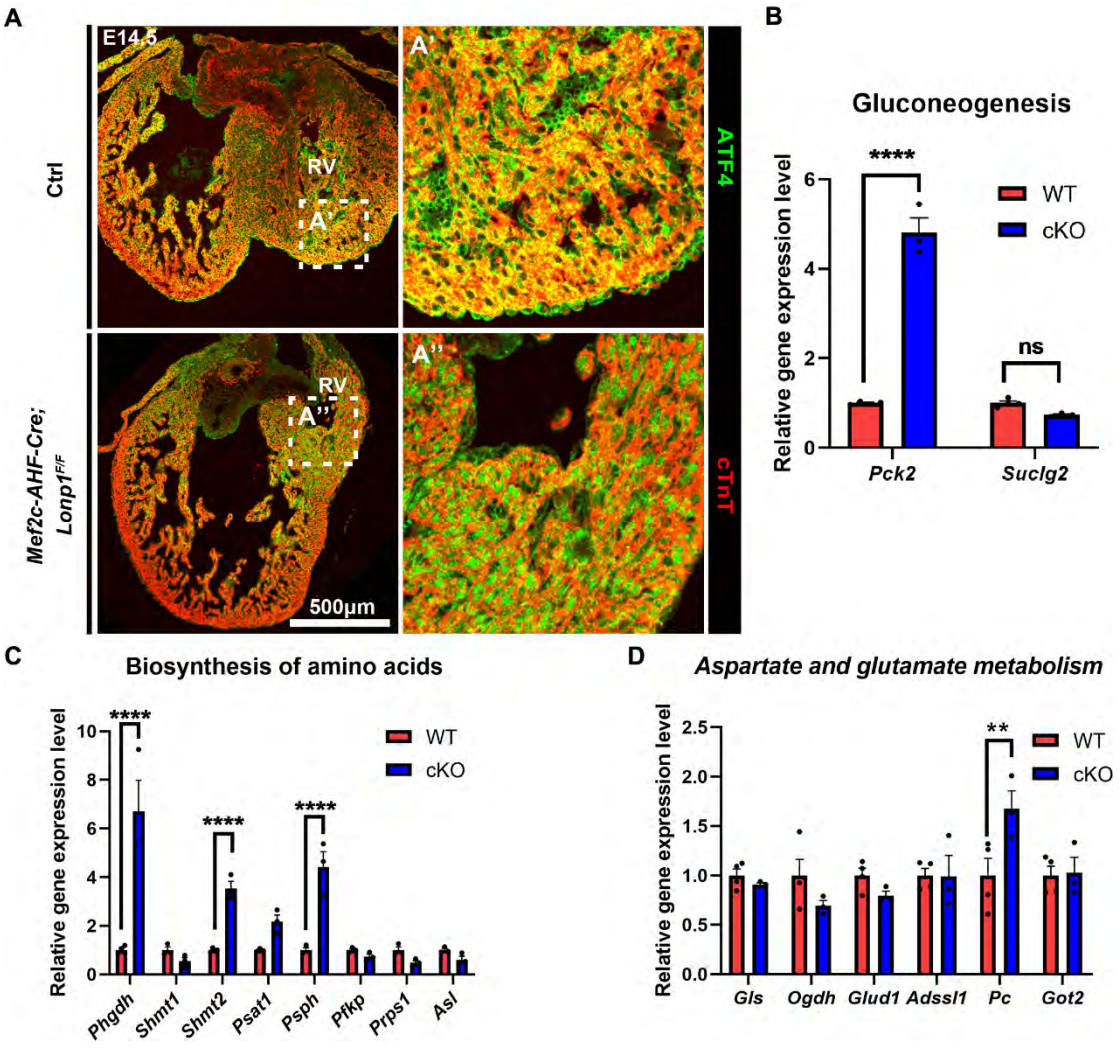

Fig. S5. Functional ATF4 was activated in the *Lonp1*-deficient heart. (**A**) IF staining shows an increase in ATF4 protein levels and nuclear localization in *Lonp1*-deficient hearts (n=3). Right panels show higher magnification of dashed box. (**B-D**) Expression of known downstream target genes regulated by ATF4 (n=3-4). Data are mean±s.e.m. ***p*<0.01, ****p*<0.001, *****p*<0.0001 (two-tailed unpaired Student's *t* test).

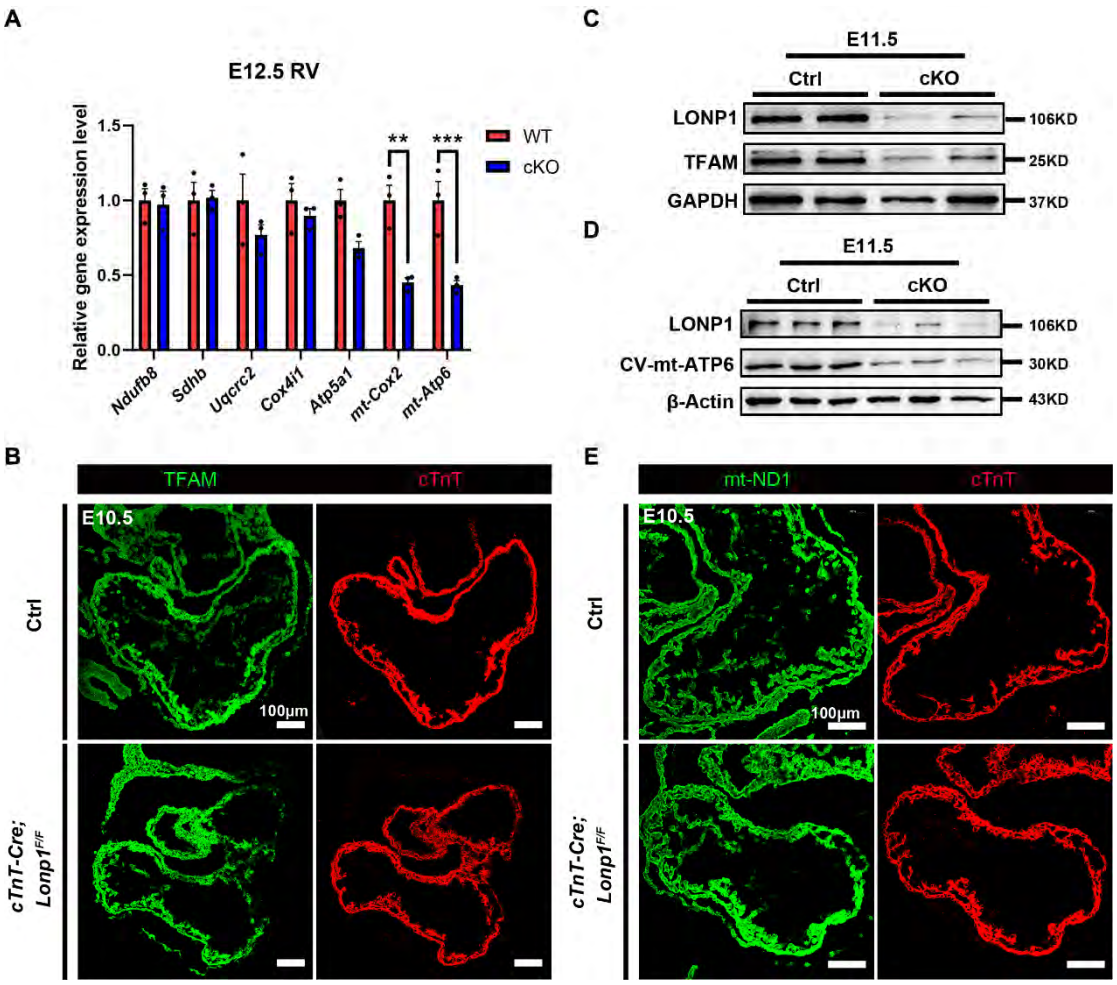

Fig. S6. *Lonp1* deficiency reduced the levels of TFAM, mtDNA and mtDNA-encoded respiratory chain complex components. (**A**) Expression of nuclear DNA and mtDNA genes encoding respiratory chain complex components in the E12.5 right ventricle. cKO is *Mef2c-AHF-Cre; Lonp1*$^{F/F}$ (n=3). (**B**) IF staining showed no significant change in TFAM levels at E10.5 (n=3). (**C**) Western blot analysis of TFAM in E11.5 hearts. cKO is *cTnT-Cre; Lonp1*$^{F/F}$. (**D**) Western blot analysis of mtDNA-encoded respiratory chain complex components in E11.5 hearts. cKO is *cTnT-Cre; Lonp1*$^{F/F}$. (**E**) IF staining showed no significant change in mtDNA-encoded respiratory chain complex component levels at E10.5 (n=3). Data are mean±s.e.m. ** p <0.01, *** p <0.001 (two-tailed unpaired Student's t test).

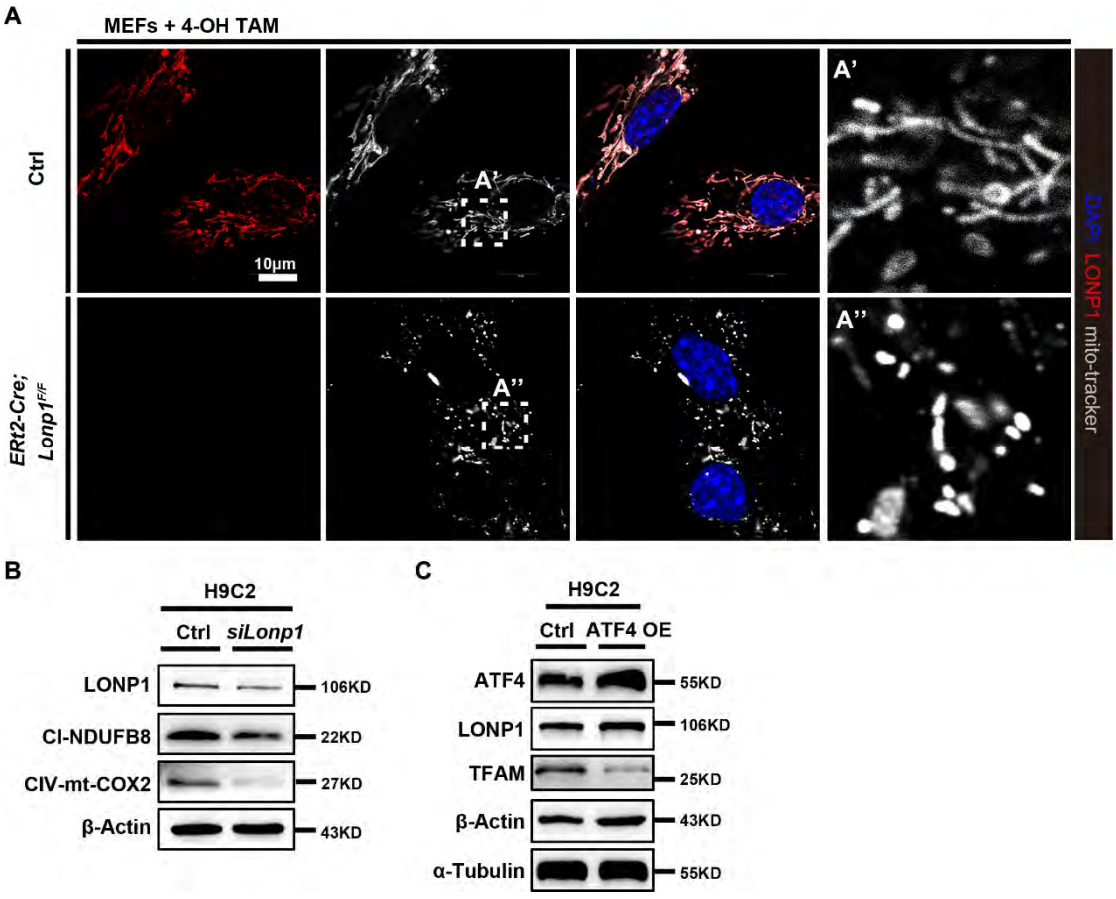

Fig. S7. Study of *Lonp1* deficient MEF cells. (**A**) IF staining showed the morphology of mitochondria in MEFs. Right panels show higher magnification of dashed box. (**B**) Western blot analysis of respiratory chain complex components in H9C2 cells. (**C**) Western blot analysis in H9C2 cells. ATF4 OE means ATF4 overexpression.

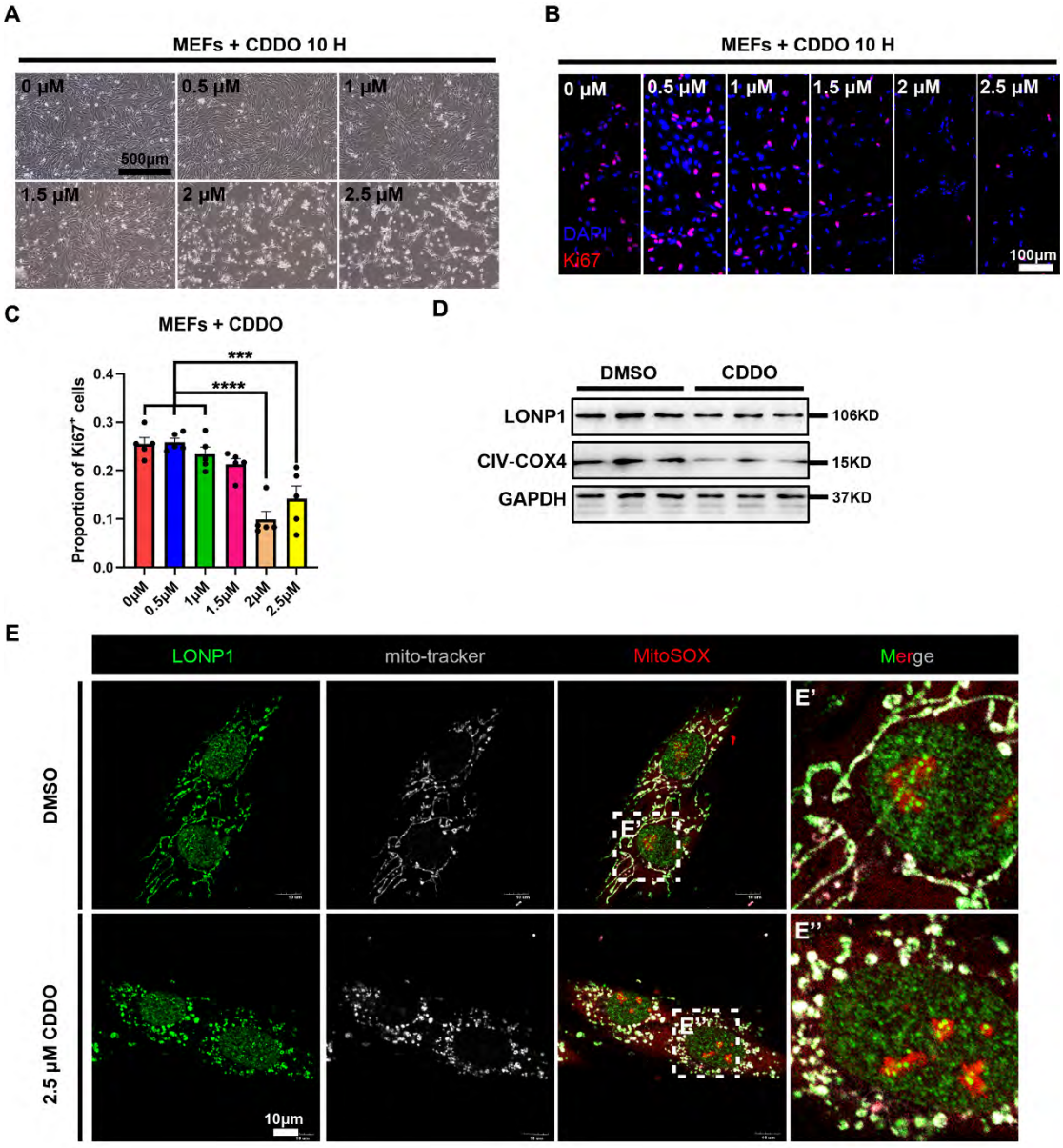

Fig. S8. CDDO treatment resulted in decreased proliferation but increased ROS *in vitro*. (**A**) Bright field images of MEFs treated with different concentrations of CDDO for 10 hours. (**B, C**) IF staining (**B**) and quantification (**C**) of proliferating MEFs. (**D**) Western blot analysis of respiratory chain complex components in MEFs treated with 2.5 μM CDDO for 10 hours (n=3). (**E**) IF staining showed the morphology of mitochondria and generation of ROS in cells. Right panels show higher magnification of dashed box. ROS marker: MitoSOX. Data are mean±s.e.m. ***p <0.001, ****p <0.0001 (one-way ANOVA).

Table S1. Primary antibodies

Antibodies	Producer	Catalog number
pHH3	CST	#9701S
ATF4	CST	#11815
AMPK	CST	#2532
p-AMPK	CST	#2535
p-eIF2α	CST	#9721
Ki67	abcam	ab15580
γH2A.X	abcam	ab11174
LONP1	abcam	ab103809
SDHB	abcam	ab178423
α-actinin	santa cruz	SC-15335
Vimentin	santa cruz	SC-5565
β -Actin	bioworld	BS6007 M
GAPDH	bioworld	AP0063
α-Tubulin	bioworld	BS1699
GLUT4	Proteintech	21048-1-AP
GLUT1	Proteintech	21829-1-AP
NDUFB8	Proteintech	14794-1-AP
eIF2α	Proteintech	11233-1-AP
UQCRC2	Proteintech	14742-1-AP
TFAM	Proteintech	22586-1-AP
ATP5a1	Proteintech	14676-1-AP
COX4	Proteintech	11242-1-AP
mt-ND1	Proteintech	19703-1-AP
mt-COX2	Proteintech	55070-1-AP
mt-ATP6	Proteintech	55313-1-ap
HK2	Proteintech	22029-1-AP
SDHA	Proteintech	14865-1-AP
Tom40	Proteintech	18409-1-AP
HSP70	Proteintech	10995-1-ap
ISL1	DSHB	40.2D6
cTnT	life	MA5-12960
CD31	BD	550274

Table S2. Primers for qRT–PCR

Gene Name	Forward primer	Reverse primer
Cdkn1a	CCTGGTGATGTCCGACCTG	CCATGAGCGCATCGCAATC
Ddit3	CTGGAAGCCTGGTATGAGGAT	CAGGGTCAAGAGTAGTGAAGGT
Atf4	CCTGAACAGCGAAGTGTTGG	TGGAGAACCCATGAGGTTTCAA
Ndufb8	TGTTGCCGGGGTCATATCCTA	AGCATCGGGTAGTCGCCATA
Sdhb	AATTTGCCATTTACCGATGGGA	AGCATCCAACACCATAGGTCC
Uqcrc2	AAAGTTGCCCCGAAGGTTAAA	GAGCATAGTTTTCCAGAGAAGCA
Cox4i1	ATTGGCAAGAGAGCCATTTCTAC	CACGCCGATCAGCGTAAGT
Atp5a1	TCTCCATGCCTCTAACACTCG	CCAGGTCAACAGACGTGTCAG
mt-Cox2	ATGGCCTACCCATTCCAACT	CGGGGTTGTTGATTTCGTC
mt-Atp6	ACACACCAAAAGGACGAACA	GAAGGAAGTGGGCAAGTGAG
mtDNA	CCTATCACCCTTGCCATCAT	GAGGCTGTTGCTTGTGTGAC
nDNA	ATGGAAAGCCTGCCATCATG	TCCTTGTTGTTCAGCATCAC
Lonp1	CGGATGTGTTTCCTCACCTG	ACGCCAACATAGGGCTGTG
Tfam	ATTCCGAAGTGTTTTTCCAGCA	TCTGAAAGTTTTGCATCTGGGT
Hif1α	GTCCCAGCTACGAAGTTACAGC	CAGTGCAGGATACACAAGGTTT
Glut1	CAGTTCGGCTATAACACTGGTG	GCCCCCGACAGAGAAGATG
Glut4	GTGACTGGAACACTGGTCCTA	CCAGCCACGTTGCATTGTAG
Hk2	TGATCGCCTGCTTATTCACGG	AACCGCCTAGAAATCTCCAGA
Pdhb	AGGAGGGAATTGAATGTGAGGT	ACTGGCTTCTATGGCTTCGAT
Ldha	TGTCTCCAGCAAAGACTACTGT	GACTGTACTTGACAATGTTGGGA
Pdk1	GGACTTCGGGTCAGTGAATGC	TCCTGAGAAGATTGTCGGGGA
Pdk4	AGGGAGGTCGAGCTGTTCTC	GGAGTGTTCACTAAGCGGTCA
Tigar	AATGTGCAGTTTACCCACGC	CTGGAGTCGTACTTCACCGC
Pck2	ATGGCTGCTATGTACCTCCC	GCGCCACAAAGTCTCGAAC
Suclg2	CCCCGAAGATGGCTGAACC	ACCTCCTTTCAAACCGCTATTG
Phgdh	ACAGCTTCGATGAAAGATGGC	TCCAAAGGATTGCATTCGGGT
Shmt1	CAGGGCTCTGTCTGATGCAC	CGTAACGCGCTCTTGTCAC
Shmt2	TGGCAAGAGATACTACGGAGG	GCAGGTCCAACCCCATGAT
Psat1	CAGTGGAGCGCCAGAATAGAA	CCTGTGCCCCTTCAAGGAG

(See table on next page.)

Psph	AGGAAGCTCTTCTGTTCAGCG	GAGCCTCTGGACTTGATCCC
Pfkp	GAAACATGAGGCGTTCTGTGT	CCCGGCACATTGTTGGAGA
Prps1	ACTTATCCCAGAAAATCGCTGAC	CCACACCCACTTTGAACAATGTA
Asl	CTATGACCGGCATCTGTGGAA	AGCAACCTTGTCCAACCCTTG
Gls	TTCGCCCTCGGAGATCCTAC	CCAAGCTAGGTAACAGACCCT
Ogdh	GTTTCTTCAAACGTGGGGTTCT	GCATGATTCCAGGGGTCTCAAA
Glud1	CCTGCAACCATGTGTTGAGC	CGGTAGCCTTCGATGACCTC
Adssl1	CTCACCTTGTGTTCGACTTCC	AGCAAAGCCCTTGAGCCTTTT
Pc	CTGAAGTTCCAAACAGTTCGAGG	CGCACGAAACACTCGGATG
Got2	GGACCTCCAGATCCCATCCT	GGTTTTCCGTTATCATCCCGGTA
TFAM	ATGGCGTTTCTCCGAAGCAT	TCCGCCCTATAAGCATCTTGA
GLUT1	GGCCAAGAGTGTGCTAAAGAA	ACAGCGTTGATGCCAGACAG
ATF4	ATGACCGAAATGAGCTTCCTG	GCTGGAGAACCCATGAGGT

Table S3. Primers for plasmid construction

Name	**Primer sequences**
m*Atf4*-pCMV7.1	F: GATGACGATGACAAGATGACCGAGATGAGC
	R: GGGGAGGGGTCACAGCGGAACTCTCTTCTT
h*ATF4*-pCMV7.1	F: GATGACGATGACAAGATGACCGAAATGAGC
	R: GGGGAGGGGTCACAGCTAGGGGACCCTTTT
m*Glut1*-2K-pGL3-Basic	F: GCGTGCTAGCCCGGGAACACTATTTCCCTG
	R: GGTGGCTTTACCAACAGGTGGGCCCGAAGG
m*Tfam*-2K-pGL3-Basic	F: GCGTGCTAGCCCGGGGCAGCATTGGCACTC
	R: GGTGGCTTTACCAACGGGCCTGGGCTGCCT